DESIGN OF A MICROFLUIDIC DEVICE FOR INDUCING CELLULAR DEFORMATION AND QUANTIFYING MIGRATION

By

JESSICA ANN COBB

A DISSERTATION PRESENTED TO THE GRADUATE SCHOOL
OF THE UNIVERSITY OF FLORIDA IN PARTIAL FULFILLMENT
OF THE REQUIREMENTS FOR THE DEGREE OF
DOCTOR OF PHILOSOPHY

UNIVERSITY OF FLORIDA

2009

To my family and my husband, Clay, for their enduring support

ACKNOWLEDGMENTS

I would like to acknowledge my doctoral supervisory committee, Dr. Z. Hugh Fan, Dr. Malisa Sarntinoranont, and Dr. Mark Segal for their guidance and support. I want to especially thank my advisor Dr. Roger Tran-Son-Tay. He encouraged me through project changes and pushed me to become the researcher that I am today.

I also want to thank the students of the Cellular Mechanics and Biorheology Lab: Rebecca Anderson (for teaching me cell culture), Cecile Perrault (for teaching me micropipette technique), Ethan Sherman (for helping with device fabrication and general brain-storming sessions), and Robert Banks (for help with diffusion simulations and compiling images). I also want to acknowledge Elaine Beem, from the Division of Nephrology, Hypertension, and Transplantation (UF), for teaching me the fundamentals of cellular migration. In addition, I thank Pan Gu from the Microfluidics and BioMEMs laboratory for fabricating the silicon wafers used for this project.

I want to thank my parents, Bob and Zona Beaty, for always believing in me and encouraging me through this long and arduous process. Most importantly, I want to thank my husband Clay for supporting me emotionally and financially for the last six years. He put his career dreams on hold so that I could pursue mine. I am forever grateful for his love and support.

TABLE OF CONTENTS

page

ACKNOWLEDGMENTS 4

LIST OF TABLES 8

LIST OF FIGURES 9

LIST OF ABBREVIATIONS 11

ABSTRACT 12

CHAPTER

1 INTRODUCTION 14

Rationale 14
Objective 15
Specific Aims 15
Relevance 15

2 BACKGROUND 17

Cellular Migration 17
Zigmond and Dunn Chambers 17
Under-Agarose Assay 19
Boyden Chamber 20
Micropipette Migration Assay 22
Micro-Scale Migration Assay/Devices 22
Cell Deformability 24
Effects of Disease on Cell Migration and Deformation 24
Jurkat Cell Migration 25
Microfabrication 25
Microfabrication Process 26
Advantages of Microelectromechanical Systems 27
Disadvantages of Microelectromechanical Systems 28

3 MATERIALS AND METHODS 35

Master Fabrication 35
Cell Culture 35
Cell Counting 35
Micropipette Experiments 35
Boyden Chamber Experiments 36
Statistical Analysis 37

4 RESULTS AND DISCUSSION 38

Specific Aim 1: Design a Microfluidic Device That Can Be Used to Induce Cell Deformation and Analyze Cell Migration 38
Micro-Device Design 38
Device layout 38
Dimensions 39
Micro-Device Fabrication 43
Casting and punching 43
Cleaning and bonding 44
Specific Aim 2: Develop the Migration Assay Protocol 45
Channel Filling 45
Cell Preparation 46
Cell Positioning and Chemoattractant Loading 46
Endpoint Quantification of Migration 48
Specific Aim 3: Test the Microfluidic Migration Device 48
Gradient Visualization 48
Observed Deformation and Migration 50
Migration Quantification Method 51
Preliminary data 53
Quantification of Jurkat cell migration 53
Chemokinesis 54
Effect of channel height on migration 56

5 CONCLUSION 75

6 FUTURE WORK 77

Compare Micro-Scale Device Results to Boyden Chamber Results 77
Reduce Variability in Micro-Device Geometry 78
Decrease Assay Time 78
Improve Micro-Device Design and Protocol 79
Alter Micro-Device Dimensions 79
Incorporate Multiple Channels into Design 79
Alter Well Geometry to Facilitate Cell Positioning 80
Automate Cell Counting 80
Automate Real-Time Analysis of Migration 80

APPENDIX

A JURKAT CELL MEASUREMENTS 83

B COMSOL MULTIPHYSICS SIMULATIONS 84

C CALCULATIONS 86

D MICRO-DEVICE DIFFUSION ANALYSIS 89

LIST OF REFERENCES 92

BIOGRAPHICAL SKETCH 96

LIST OF TABLES

Table page

4-1 Microscale migration device dimensions....58

A-1 Measured diameters for Jurkat cells 83

D-1 Diffusion simulation results for micro-scale device with varied dimensions....89

LIST OF FIGURES

Figure		page
2-1	Cell migration schematic.	29
2-2	Zigmond chamber	30
2-3	Dunn chamber	30
2-4	Under-agarose/ECIS assay schematic	31
2-5	Boyden chamber schematic.	31
2-6	Microfluidic gradient generator designed by Li et al	32
2-7	Microfluidic migration device designed by Shamloo et al	32
2-8	Schematic representing the “Ladder chamber” designed by Saadi et al	33
2-9	Schematic representing the “KK-Chamber” designed by Kanegasaki et al	33
2-10	Photolithography process schematic	34
2-11	Schematic detailing silicon etch profiles	34
4-1	Micro-scale migration device schematic	58
4-2	Simulated concentration gradient within a microchannel of uniform depth	59
4-3	Schematic of micro-scale migration device with cell holding chamber (CHC)	59
4-4	Simulated concentration gradient within a device with a CHC.	60
4-5	Effect of CHC length on gradient	61
4-6	Diffusion simulation demonstrating presence of gradient up to 7 days	62
4-7	Schematic showing media reservoir fitted on top of micro-device.	62
4-8	Microchannel filled with fluorescent dye.	63
4-9	Jurkat cells positioned within CHC.	63
4-10	Jurkat cells stained within the chemoattractant (CA) well.	64
4-11	Fluorescein isothiocyanate (FITC)-dextran solution in the micro-device	64
4-12	Gradient visualization using FITC-dextran.	65

4-13 Jurkat cells migrating through the microchannel 66
4-14 Micro-device divided into cell counting zones 67
4-15 Results for Jurkat cell migration in Boyden chamber 68
4-16 Effect of stromal cell-derived factor-1 (SDF-1) concentration on the migration ratio 69
4-17 Effect of channel length on migration ratio in micro-devices 70
4-18 Boyden migration ratios for Jurkat cell “net migration” and “chemokinesis.” 71
4-19 Chemokinesis (100 nM SDF-1) test performed in micro-device 72
4-20 Jurkat cell migration ratios for 14, 10, and 8 μm channel heights 73
4-21 Jurkat cell migration experiment performed in device with channel height = 8 μm 74
6-1 Schematic of altered cell well geometry 82
B-1 Schematic and parameter inputs used for Comsol Multiphysics 84
B-2 Representative Comsol Multiphysics output 85
B-3 Plot of concentration versus distance from the CA well 85
C-1 Schematic illustrating force calculations within the micro-device 86

LIST OF ABBREVIATIONS

CA	Chemoattractant
CHC	Cell holding chamber
DI	Deionized
ECIS	Electric cell impedance sensing
FITC	Fluorescein isothiocyanate
FBS	Fetal bovine serum
HBSS	Hanks' balanced salt solution
HMDS	Hexamethyldisilazane
MEMs	Microelectromechanical systems
MR_{Boyden}	Migration ratio for Boyden chamber
MR_{exp}	Migration ratio for micro-device, experimental method
MR_{micro}	Migration ratio for micro-device
MW	Molecular weight
PBS	Phosphate buffered saline
PDMS	Poly(dimethylsiloxane)
S-184	Slygard® 184
SDF-1	Stromal cell-derived factor-1
SCM	Serum-containing RPMI 1640 media
SFM	Serum-free RPMI 1640 media
T-2	Silastic® T-2 RTV

Abstract of Dissertation Presented to the Graduate School
of the University of Florida in Partial Fulfillment of the
Requirements for the Degree of Doctor of Philosophy

DESIGN OF A MICROFLUIDIC DEVICE FOR INDUCING CELLULAR DEFORMATION AND QUANTIFYING MIGRATION

By

Jessica Ann Cobb

December 2009

Chair: Roger Tran-Son-Tay
Major: Biomedical Engineering

Cellular migration is fundamental to various biological processes including embryogenesis, angiogenesis, immune response, wound healing, and cancer metastasis, among others. As a result, methods for studying migration are key for developing therapies that promote health and battle disease. In the past, various migration assays have been developed. The advantageous features among these assays are as follows: low volume requirement of costly chemicals, cell deformation to mimic migration through tissues *in vivo*, the means to observe migration in real-time, and a method for quantifying migration. None of the previous assays integrated all of these elements. Therefore, the goal of this project was to develop a migration assay that incorporates all of the advantageous features.

A microfluidic cellular migration device was designed, fabricated, and tested using white blood cells. The micro-scale dimensions of the device forced the cells to deform in order to migrate and reduced the volume of chemicals required by a factor of 10. The chemical gradient that drives migration was generated in the device within 5 minutes and was maintained for at least 7 days. The device was made of a transparent material making it suitable for real-time migration analysis via microscopy. In addition, a technique was developed to stain the cells within the device in order to quantify migration.

The micro-scale migration device can be used to study the migration mechanics of individual cells. In addition, it can be used to quantify and compare the migration of multiple cell populations. As a result, it has wide spread applications in various fields of study including, but not limited to cell rheology, immunology, wound healing, cancer metastasis, and drug discovery.

CHAPTER 1
INTRODUCTION

The process of cellular migration is fundamental to human life beginning with embryogenesis and continuing throughout life in numerous processes such as immune response and wound healing. In addition to starting and sustaining life, migration plays a role in pathological conditions such as vascular disease, chronic inflammatory diseases, and tumor formation and metastasis, among others[1]. As a result, methods for studying cell migration are critical for developing effective therapies.

Rationale

Various devices have been used over the last century to study cellular migration. Migration on flat surfaces, between two flat surfaces, and through filters are some of the configurations that have been used. The drawbacks of these designs include difficulty of use, lengthy assay times, large volume requirements of costly reagents, and poor result reproducibility. In addition, most lack a method for quantifying migration. More recently, micro-scale devices have been designed which decrease assay time by decreasing the volume of reagents used, thereby reducing assay cost as well. However, like their predecessors they can be tedious to operate, prone to poor reproducibility, and they do not quantify migration.

An additional drawback of most cell migration assays to date is the lack of cell deformation during the migration process. Cells must deform to migrate through tissues *in vivo*. There is a limited number of existing migration assays that force cells to deform in order to migrate. While these do incorporate this critical feature they still suffer from some of the other disadvantages mentioned previously. As a result, a novel design that addresses these drawbacks and induces deformation is needed to accurately assess migratory function.

Objective

The objective of this project was to develop a microfluidic cellular migration device that can be used to induce cell deformation and analyze migration in real-time, as well as provide an endpoint quantification of migration.

Specific Aims

1. Design a microfluidic device that can be used to induce cell deformation and analyze cell migration

    a) Identify the parameters required to develop a micro-scale migration device
    b) Choose device dimensions
    c) Optimize device fabrication protocol

2. Develop the migration assay protocol

    a) Optimize micro-channel filling
    b) Optimize cell positioning
    c) Optimize chemoattractant loading
    d) Develop a protocol for quantifying migration

3. Test the microfluidic cell migration device

    a) Use fluorescence microscopy to visualize gradient formation and maintenance within the micro-scale migration device

    b) Monitor assay via microscopy to ensure cells are deforming and migrating in the device

    c) Use the micro-scale device to quantify migration of white blood cells

    d) Alter the channel height in the micro-scale migration device to evaluate the effect that deformation has on migration

Relevance

The micro-scale dimensions of the migration device developed for this project significantly reduce the volume of costly chemicals required to study cellular migration. Reducing the expense of each assay allows for additional studies to be conducted, thereby leading to greater scientific discovery. In addition, this device forces cells to deform in order to migrate. This provides more physiologically relevant data than methods that measure migration

without deformation. Furthermore, this device allows for real-time analysis of migration as well as an endpoint quantification of migration. Other migration devices fail to incorporate both of these features. All of the features integrated in this design make up a superior cellular migration device that can be used to advance diagnostic and therapeutic applications in the medical field.

CHAPTER 2
BACKGROUND

Cellular Migration

Cells move in response to external stimuli (chemical agents). Chemokinetic agents promote random cell movement, while chemotactic agents (soluble chemicals) and haptotactic agents (substrates) promote directed cell movement (chemotaxis). Migration is a cyclical process that begins when a cell senses one of these agents, polarizes, and extends a protrusion (by polymerizing actin) in the direction of movement (see Figure 2-1). The protrusion attaches to the substratum via adhesion complexes composed of integrins, kinases, and several other adaptor and structural molecules. This is followed by actin-myosin mediated contraction that moves the cell forward. Finally, adhesion complexes in the rear of the cell are released, the tail retracts, and another protrusion is extended to continue movement in the direction of the chemoattractant[1].

The first observation of chemotaxis was on leukocytes in 1888[2]. Since then various methods have been developed and employed for studying this phenomenon. Simple techniques include the direct visualization of cell chemotaxis in capillary tubes[3] and between a slide and coverslip[4]. More intricate techniques utilize separate wells, layers of agarose, filters, and flow-based devices.

Zigmond and Dunn Chambers

The Zigmond chamber is used to directly observe chemotaxis via video microscopy. The chamber consists of two linear wells separated by a bridge (Figure 2-2A). Cells are seeded onto a coverslip. Once the cells have attached to the coverslip it is inverted, placed on top of the wells, and held in place with clamps on both sides of the chamber (Figure 2-2B). Control medium (which contains no serum) is placed in one well and the chemoattractant is placed in the

other well. The chemical gradient that forms between the bridge and overlying coverslip (10 to 20 μm gap) drives the cells to migrate. Migration is viewed and captured with video microscopy[5, 6].

Since it is made of glass, the Zigmond chamber has ideal optical properties for microscopy. Video microscopy allows for the direct observation of migration and the use of cell-tracking software. While this can provide valuable real-time information, it monopolizes a microscope for the duration of the experiment, thereby limiting the number of chambers that can be used simultaneously. An additional drawback for this device is poor reproducibility of its dimensions[6]. The clamps cause flexure of the coverslip, which varies between experiments due to differences in clamp tightness. Variations in coverslip flexure produce variations in the gap width between the bridge and coverslip. As a result, gradient establishment and decay vary, producing disparities in experimental results. In addition, assembling the chamber without producing bubbles in the fluid (which affect the gradient) is difficult and takes a lot of practice. Another disadvantage of this chamber is the lack of induced cell deformation, an integral component of the migration process. Other limitations include the large volume requirement (>100 μl) of expensive chemicals, the small number of cells that can be analyzed at one time (since each device only contains one migration chamber), and the length of the assay. It takes several hours for the cells to attach to the coverslip before the experiment can be started. Once the chamber has been assembled it typically takes 1 hour or more for the gradient to be established and then several hours (4 to 24) for migration to occur. The length of this assay necessitates a sterile environment around the microscope, a stage incubator, and CO_2 independent cell culture media.

The Dunn chamber is similar to the Zigmond chamber. It consists of two wells separated by a bridge, and allows for direct observation of migration through video microscopy. It differs in its layout. The Dunn chamber contains two concentric circular wells separated by an annular bridge (Figure 2-3A). Control medium is placed in the center well, while the chemoattractant is placed in the outer well. Cells are seeded onto and allowed to attach to a coverslip which is then inverted and placed on top of the wells (leaving a portion of the outer well open for loading). It is sealed in place with wax (Figure 2-3B). The gap between the coverslip and the bridge is typically ~20 μm[7]. Video microscopy is used to observe migration across the bridge[5, 6].

As with the Zigmond chamber, the Dunn chamber has good optical properties for microscopy and cell-tracking software. In contrast to the Zigmond chamber, the Dunn chamber has precise and reproducible geometry. Instead of clamps, it uses wax to attach the coverslip. This does not cause significant variations in coverslip flexure. In addition, the concentric layout of the bridge and wells make the chamber less prone to flexure, provides a more positive seating for the coverslip, and avoids the end effects associated with a linear bridge. This provides good gradient reproducibility, and thus, reproducible results[6]. Similar to the Zigmond chamber, the Dunn chamber is difficult to assemble without introducing bubbles, does not induce cell deformation, requires a large volume of chemicals, only has one migration chamber which limits the quantity of cells that can be analyzed at one time, is a lengthy assay, and monopolizes lab equipment. In addition, neither the Dunn nor Zigmond chambers can be used to study suspension cells since they will not attach to the coverslip.

Under-Agarose Assay

The under-agarose assay measures cell migration under a layer of agarose toward a well that contains a chemoattractant source. In the past this has been done in ordinary cell culture

dishes. Once the experimental time has elapsed fixative is added to the dish, the agarose is removed, the culture dish is stained, and cell migration is analyzed via microscopy[8, 9]. More recently this technique has been updated with an electric cell impedance sensing (ECIS) system that automatically monitors cell migration[5]. In the under-agarose/ECIS assay each well contains a large common electrode and a smaller target electrode. Agarose is laid down within the wells covering the electrodes. After it has set, wells are punched into the agarose on either side of the target electrode. Chemoattractant is placed in one of the wells and given approximately one hour for a gradient to form within the agarose. The cells of interest are then placed in the well on the other side of the target electrode. The cells migrate under the agarose toward the higher concentration of the chemotactic source. As they migrate they cross over the target electrode, increasing resistance within the circuit (Figure 2-4). Resistance values are proportional to the number of cells present on the electrode at any given time. Video microscopy is used to get an initial correlation between the resistance values and the number of cells on the electrode.

The under-agarose/ECIS assay monitors the movement of cells throughout the course of the assay showing real time cell response. Another advantage of this assay is its ability to analyze migration through multiple chemotactic fields (by increasing the number of wells and chemoattractants used). Disadvantages include poor reproducibility of dimensions (gap between agarose and the well bottom) and length of the assay (6 hours or more). Furthermore, some cell types (e.g. lymphocytes) typically do not migrate under the agarose.

Boyden Chamber

The Boyden chamber is the most commonly used migration assay. It indirectly evaluates chemotaxis by quantifying migration through a micro-porous filter. The filter separates each chamber into an upper and lower well (Figure 2-5). The chemoattractant is placed in the lower well while the cells of interest are placed in the upper well. Through the course of the assay cells

migrate down through the filter toward the higher concentration of chemoattractant. Afterwards the filter is removed, the underside is stained, and the cells are counted[10]. An alternative method of enumeration involves the fluorescent labeling of the cells prior to being loaded into the chamber. After the assay is completed the amount of fluorescence in the lower wells of positive (with chemoattractant) and negative (no chemoattractant) controls are compared to obtain the percentage of cells that migrated through the filter.

There are various filter pore sizes available for commercially produced Boyden chamber systems (2 to 14 μm)[11], therefore, a wide range of different cell types can be studied with these devices. The pore size that is used should be based on the cell type being used. More specifically, the pore size should be smaller than the cells of interest so that deformation during migration occurs. This mimics *in vivo* migration. Another advantage of the Boyden chamber is multiple wells within each device. Multiple chambers allow serial quantification of chemotaxis under a range of different conditions. A drawback of the Boyden chamber is that it is very difficult to properly assemble. It must be loaded and assembled without creating bubbles, which affect the gradient and inhibit migration. Other disadvantages include a large volume requirement of chemicals (up to 245 μL per well for some commercially available Boyden chambers), poor reproducibility, a steep gradient that rapidly dissipates, and it requires a large number of cells to obtain a statistically significant cell migration count. In addition, the movement of cells through the filter cannot be observed, and cells can obstruct pores within the filter modifying the local concentration gradient and altering the paths of other cells that could have passed through those pores.

Micropipette Migration Assay

Micropipette systems have been used to study cell migration. Chemoattractants introduced into the distal end of the pipette induce chemotaxis and the cell deforms and enters the proximal end of the pipette[12, 13]. This method can be used to measure migration parameters of individual cells. While this can be an advantage, this method is not generally used because it is difficult to manipulate the micropipettes. In addition, the low throughput of this device makes it unsuitable for many applications.

Micro-Scale Migration Assay/Devices

Within the past decade microfluidic technology has been applied to cell migration research. Micro-scale devices have the advantage of using significantly smaller volumes, which decrease the amount of costly reagents and the number of cells that are required. Various designs for micro-scale migration devices can be found in the published literature. Elegant designs consist of a source and sink connected by a single channel or multiple channels in parallel[14, 15]. More intricate designs utilize micro-valves to open and close various channels/chambers, thereby generating chemical gradients[16, 17].

Many of the micro-scale migration devices use continuous flow in order to maintain the chemical gradient for extended periods of time. The most prominent of the flow-based devices is the microfluidic gradient generator (Figure 2-6) created by Li and colleagues[18]. This device contains multiple branched channels that combine, mix, and split fluid streams in order to create different gradient shapes. The advantage of this design is its ability to create gradients almost instantaneously, and maintain them indefinitely. The gradient generator has been used to study the migration of white blood cells[18-20] and cancer cells[21, 22], among others. Shamloo et al.[23] (Figure 2-7) and Cheng et al.[24] designed devices that utilize flow in source and sink channels that are connected to a central cell culture channel. The micro-capillaries that connect the three

channels are small enough to prevent fluid flow within the cell channel. As a result, the cells migrate in response to the gradient formed via diffusion in the capillaries.

While the use of flow within migration devices has advantages, it also has drawbacks. Flow disrupts cell signaling which can affect migration behavior. *In vivo*, cells secrete autocrine (self signaling) and paracrine (cell-cell signaling) factors that help to regulate migration. In flow-based devices these factors are immediately washed away, thereby disrupting cell signaling[14, 15]. An additional concern is the biased cell movement that results from flow. Walker and colleagues showed that cells migrated further downstream as flow rate within a microfluidic device was increased[25]. This makes it impossible to separate the effects of chemotaxis and fluid flow on cell migration. Finally, flow based devices are economically disadvantageous. They require additional equipment to maintain flow (i.e. pumps) and utilize larger volumes of costly reagents because they constantly have to be replenished to maintain the gradient.

Most of the micro-scale devices previously mentioned have channel dimensions that are larger than the cells that migrate through them. As a result, they do not induce cell deformation. Conversely, there are a few devices that do force cells to deform in order to migrate. Saadi et al.[15] developed the "Ladder Chamber" which consists of several microgrooves in parallel that connect a source and sink channel (Figure 2-8). Cells must deform to traverse the microgrooves (height < 10 μm). Despite this advantageous feature, the device uses continuous flow in the source and sink channels. Chaw et al.[26, 27] designed a device with microgaps (width = 10 μm) through which single cells deform and migrate. Whereas this allows for detailed assessment of single cells it does not permit high throughput. Furthermore, this assay takes several days to complete. Kanegasaki et al.[28] designed the "KK-Chamber" (also known as "TAXIScan"[29]), which consists of two wells connected by a microchannel (height = 5 μm) through which cells

deform and migrate (Figure 2-9). The drawback for this device, as well as for all the other microscale devices is the lack of endpoint quantification. These devices allow direct visualization of cell migration but do not provide an end value that can be used to compare the results from various experiments.

Cell Deformability

Cells must deform to migrate through tissues in the body. A cell's ability to deform is a function of its cortical tension and cytoplasmic viscosity. Cortical tension is imparted by the cell's cytoskeleton. The cytoskeleton is composed of actin filaments, microtubules, intermediate filaments, and other proteins that control the growth, cross-linking, and attachment of the filaments to the cell membrane. Cellular deformation and migration are carried out by all of these proteins working together[30]. The cytoplasm of a cell contains water, macromolecules, metabolites, and ions. Needham and Hochmuth[31] showed that the cytoplasm of some cells (e.g. white blood cells) behaves as a Newtonian fluid, meaning its viscosity remains constant at a given temperature, regardless of the rate of shear.

Micropipette aspiration and recovery experiments[32] can be used to measure cytoplasmic viscosity and cortical tension. Briefly, a cell is aspirated into a pipette of lesser diameter under constant pressure. The cell will behave as a Newtonian fluid and flow into the pipette in a time-dependent manner. After being fully aspirated, the cell is expelled and allowed to recover its spherical shape. Measurements are taken throughout the aspiration and recovery processes and used to calculate the cell's cytoplasmic viscosity[31] and cortical tension[33].

Effects of Disease on Cell Migration and Deformation

Various studies have shown mechanical differences between healthy and diseased cells. The micropipette technique has been used to show decreased deformability of white blood cells[34-36], erythrocytes from patients with sickle cell disease[37] and diabetes[36], and various cancer

cells[38, 39]. Segal and colleagues[40] compared the migration rates of CD34+ cells isolated from diabetic patients and healthy volunteers. They showed that in response to the chemokine stromal cell-derived factor -1 (SDF-1), diabetic CD34+ cells exhibited just 30% of the maximal migratory activity of healthy CD34+ cells. In addition, micropipette experiments showed that the diabetic CD34+ cells were more rigid than their healthy counterparts. None of the diabetic CD34+ cells deformed (none of the cells could be suctioned into the pipette), while the majority of the healthy cells deformed and entered the pipette (75% of the cells completely entered, 16.7% partially entered, and 8.3% did not enter at all). Incubation with nitric oxide increased the deformability and migration rates of the diabetic cells. Based on the known fact that nitric oxide affects the cytoskeleton, this suggests that cytoskeletal defects exist in diabetic CD34+ cells making them more rigid and less able to migrate than healthy CD34+ cells.

Jurkat Cell Migration

Jurkat cells are an immortalized T lymphocyte cell line. Stromal cell-derived factor-1 is a chemokine that signals cell migration[41]. The SDF-1 receptor CXCR4 is expressed on the surface of Jurkat cells. As a result, Jurkat cells migrate in the presence of an SDF-1 gradient[42].

Microfabrication

Microelectromechanical systems (MEMS) are miniaturized devices that have dimensions that range from micrometers to millimeters. MEMs technology began several decades ago when semiconductor fabrication technology was modified to incorporate electrical and mechanical processes onto small silicon chips. More recently MEMs and biology have merged creating BioMEMs which includes miniaturized versions of various biological assays. For instance, polymerase chain reaction (PCR), DNA separations, and cell sorting are just a few of the techniques that have successfully been integrated into BioMEMs. These assays often require several steps such as incubations and mixing, which are possible due to the incorporation of

valves, pumps, and separate chambers within the micro-devices. Given that these devices can perform many assays from start to finish they are often referred to as "Lab-on-a-chip" devices[43].

Microfabrication Process

There are numerous microfabrication processes that are detailed in the literature[43, 44]. A brief overview of the methods used for this project is given here. Soft lithography is the process used to create microchannels in poly(dimethylsiloxane) (PDMS). This technniqe begins by making a *mask* that contains the desired channel pattern. The pattern is transferred to a silicon wafer through a photolithography process and subsequently etched into the wafer. The wafer is then used to generate patterned PDMS pieces that are bonded to glass to create microchannels.

The desired channel pattern is drawn with a CAD program. Next, it is transferred to the mask material. Masks can be made by depositing a thin layer of chrome (in the desired pattern) onto a glass plate, or by transferring the pattern to photographic film creating a photomask.

Photolithography is the process by which the pattern on the mask is transferred to the wafer. First, the wafer substrate (usually silicon) is spin coated with photoresist, a photosensitive polymer. There are two types of photoresist, positive and negative. When positive photoresist is exposed to UV light it becomes more soluble in developing solution. Conversely, negative photoresist becomes less soluble in developing solution upon UV exposure. When the mask and substrate are aligned UV light is shown through the transparent portions of the mask chemically altering the photoresist to create the pattern (Figure 2-10). Next, the substrate is submersed in developing solution which removes any soluble photoresist, thereby exposing the substrate for etching.

The pattern is chemically carved into the substrate by wet etching or dry etching. Wet etching consists of submersing the wafer in liquid chemicals, while dry etching is done by

exposing the wafer to gases. Dry etching is used to create tighter patterns and is more expensive than wet etching.

There are two different types of etch profiles, isotropic and anisotropic. As shown in Figure 2-11 isotropic etching etches equally in all directions giving a rounded profile that often undercuts the mask. Conversely, anisotropic etching is direction-dependent and creates more controlled features (Figure 2-11). Both wet etching and dry etching can be used to generate isotropic or anisotropic profiles, however, anisotropic etching is most often done with dry etching. The substrate material properties, etchant selectivity, and desired etch rate and profile must be considered when choosing an appropriate etchant. For example, wet etching [100] single-crystal silicon with potassium hydroxide creates a profile with a 54.7 º angle with the horizontal (Figure 2-11).

The patterned wafer, also known as the *master*, is used for rapid prototyping. PDMS is one of the most commonly used materials in rapid prototyping for biological applications. It is inexpensive and easy to use. It is mixed up as a liquid, poured onto the master, cured, and peeled off the master without damaging its surface. It is optically transparent making it suitable for microscopy. In addition, it is biocompatible and biochemically inert, making it appropriate for biological applications[45].

There are various bonding techniques that can be used to fabricate micro-devices. The reader is referred to the literature[43, 44] for details on each technique. For this project, microchannels were formed by bonding the patterned PDMS pieces to glass slides.

Advantages of Microelectromechanical Systems

Micro-scale devices have many advantages over their conventional counterparts[43]. They are portable, take up less space, and have high throughput because many channels can operate in parallel. The volume requirement is less; therefore, the use of costly reagents and scarce samples

is decreased. In addition, the decreased volume reduces reaction times, which can shorten assay time. Also, the surface area-to-volume ratio is increased in micro-devices, thereby enhancing heat removal, which is critical for devices that utilize electric fields. Another advantage given to electrical micro-devices is a decrease in the voltage required to create gradients of the same strength in macro-scale devices. Finally, micro-scale dimensions make single-cell analysis more feasible.

Disadvantages of Microelectromechanical Systems

Micro-scale devices are generally more expensive and take longer to manufacture than their conventional counterparts. The increased surface area-to-volume ratio increases surface adsorption of biomolecules and ultimately lowers yield. Also, the small volumes can evaporate rapidly if no measures are taken to prevent it. Despite these drawbacks, micro-scale devices are often preferred over their macro-scale counterparts due to the advantages previously mentioned[43].

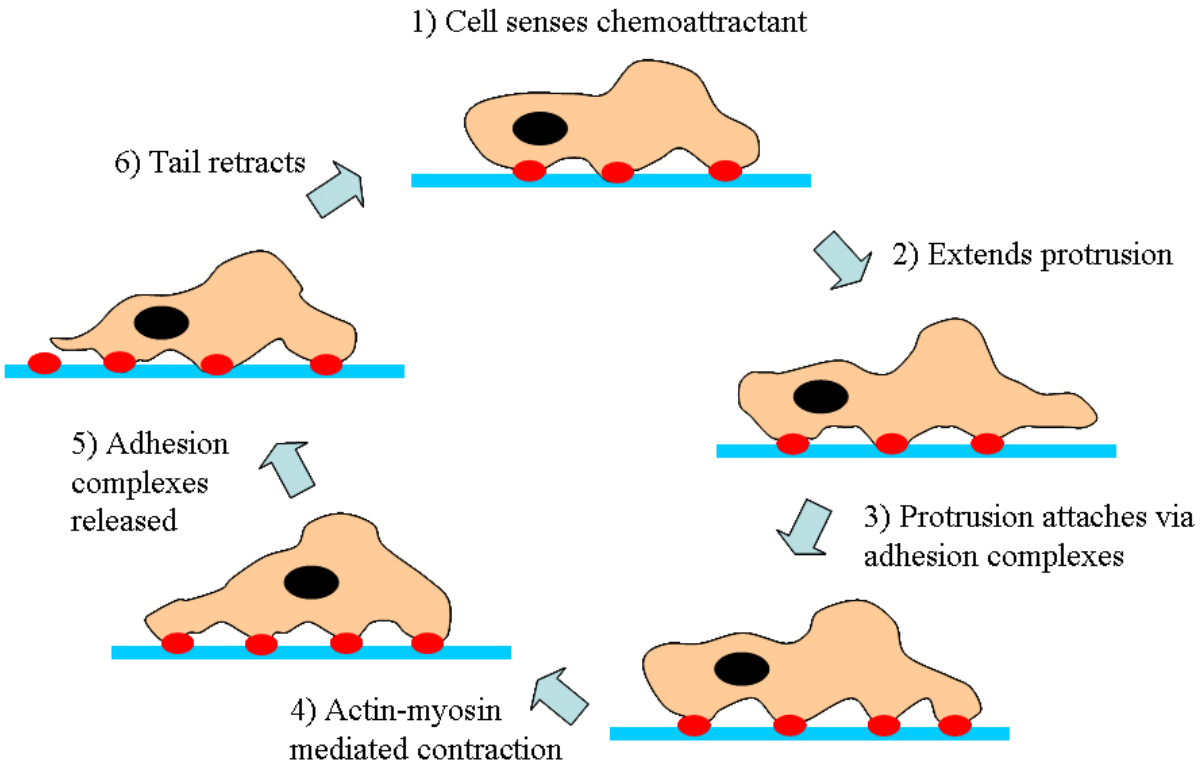

Figure 2-1. Cell migration schematic.

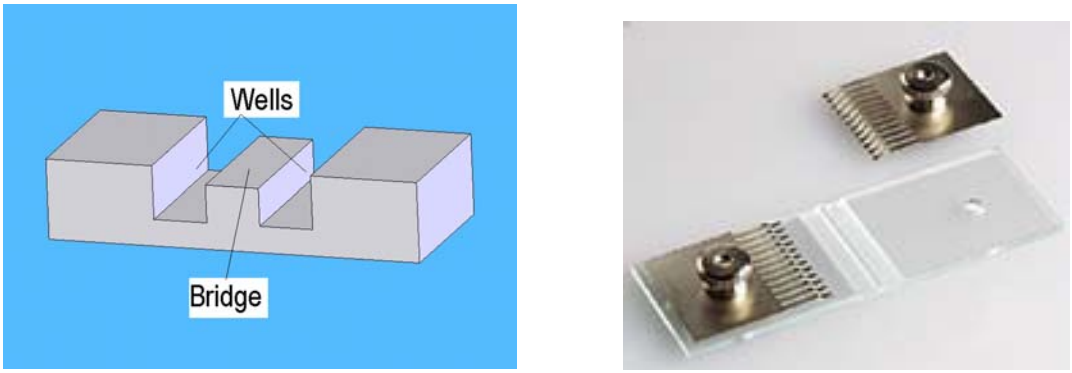

A B

Figure 2-2. Zigmond chamber A) schematic, and B) commercially available Zigmond chamber (image reproduced with permission from Neuro Probe, Inc.: www.neuroprobe.com).

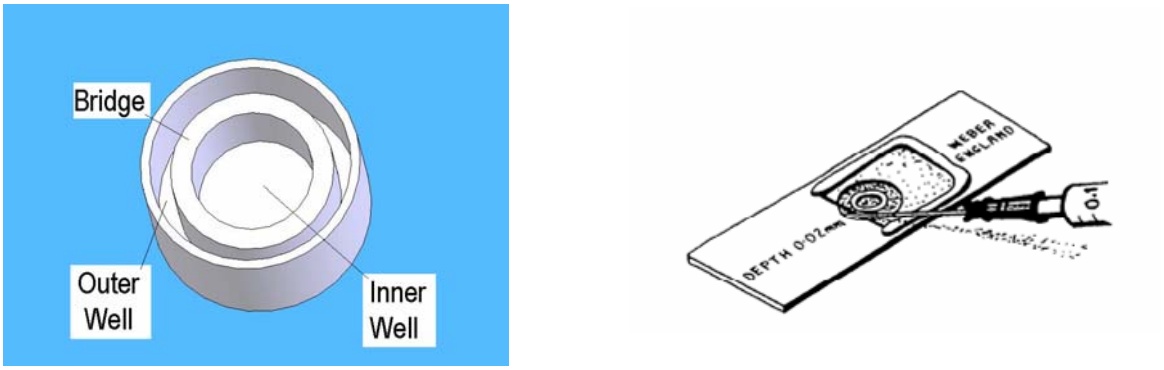

A B

Figure 2-3. Dunn chamber A) schematic and B) Dunn chamber with wax holding coverslip in place (image reproduced from: Zicha et al. *Journal of Cell Science* 1991;99:769-775, with permission from The Company of Biologists).

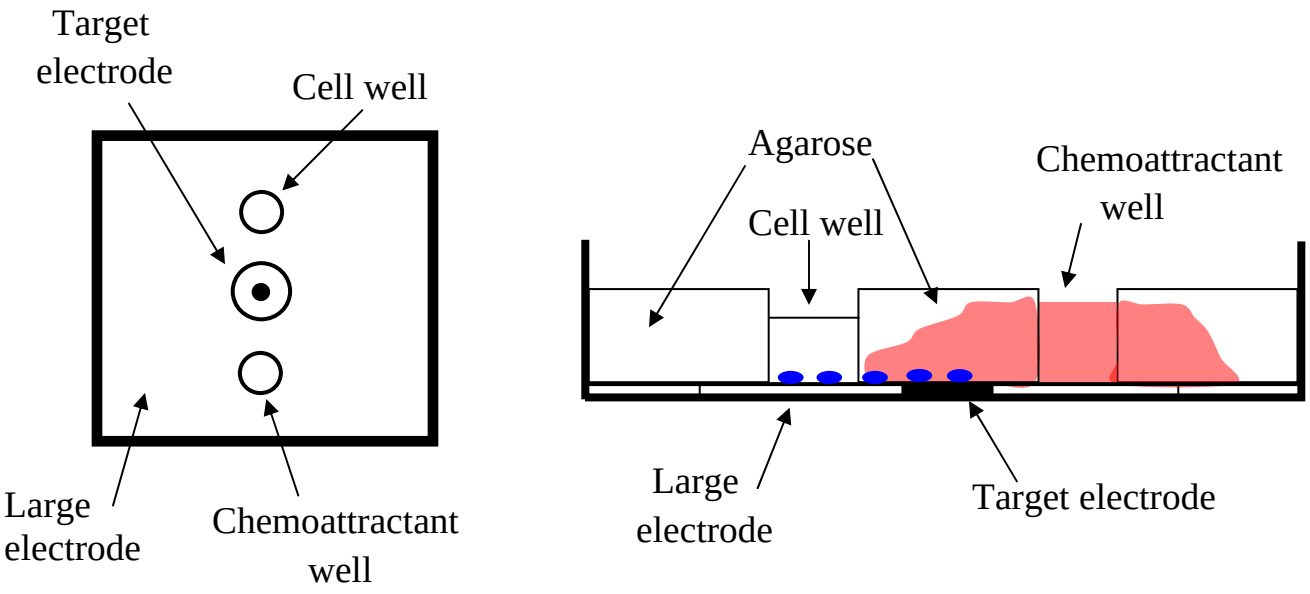

Figure 2-4. Under-agarose/ECIS assay schematic. A) top view of electrode, B) side view of chamber showing the chemoattractant diffusing through the agarose and the cells migrating across the target electrode.

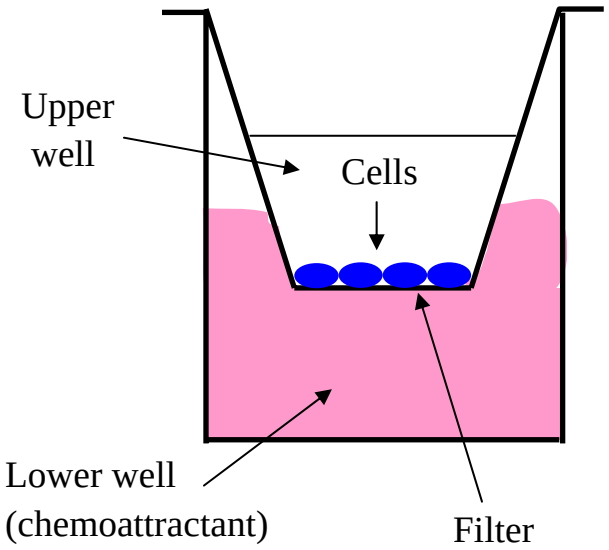

Figure 2-5. Boyden chamber schematic.

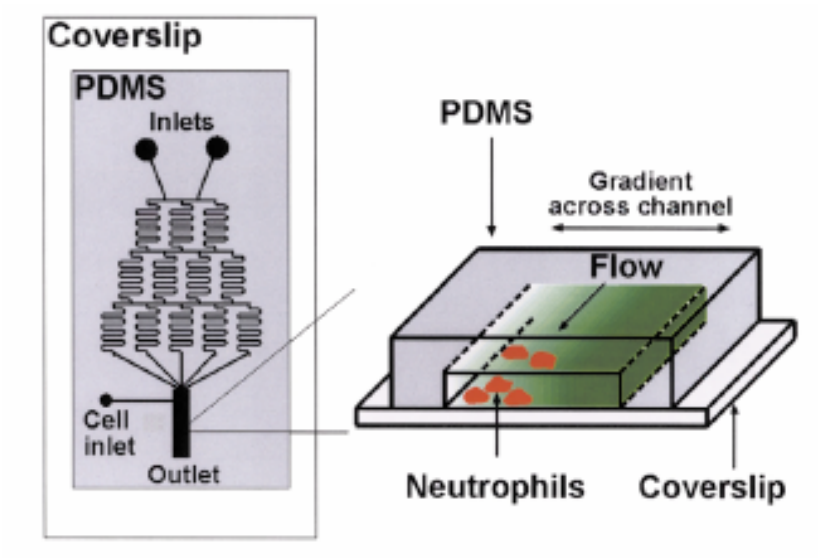

Figure 2-6. Microfluidic gradient generator designed by Li et al. Image reprinted by permission from Macmillan Publishers Ltd: Nature Biotechnology 20(8):826-830 (2002).

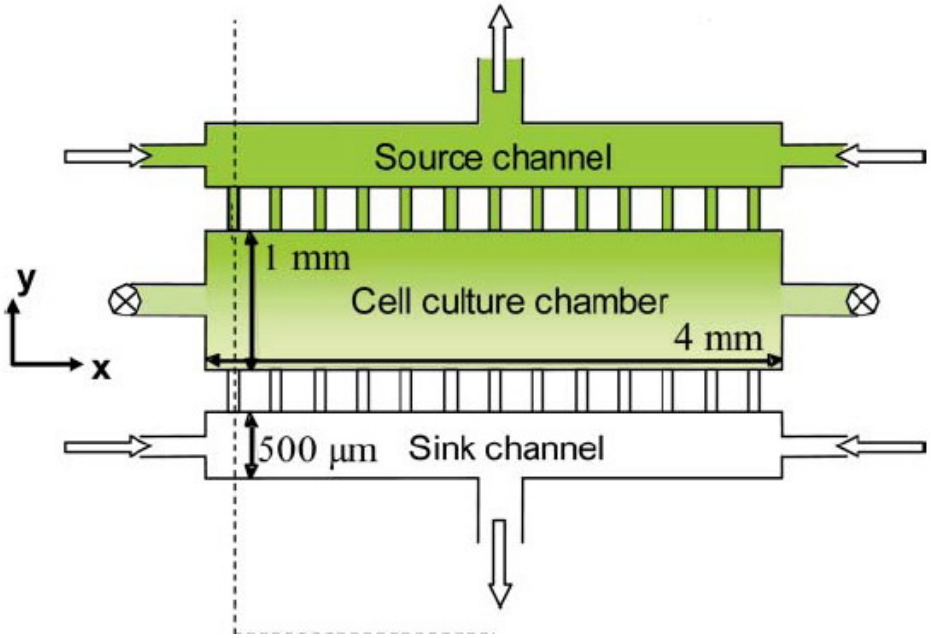

Figure 2-7. Microfluidic migration device designed by Shamloo et al. (2008) Lab on a Chip 8:1292-1299-reproduced by permission of the Royal Society of Chemistry.

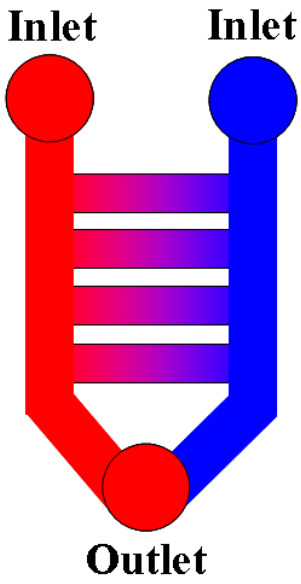

Figure 2-8. Schematic representing the “Ladder chamber” designed by Saadi et al. (2007).

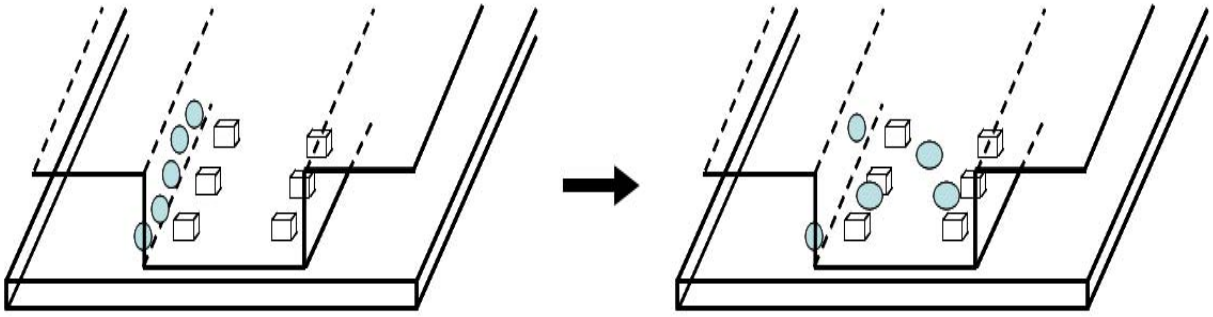

Figure 2-9. Schematic representing the “KK-Chamber” designed by Kanegasaki et al. (2003).

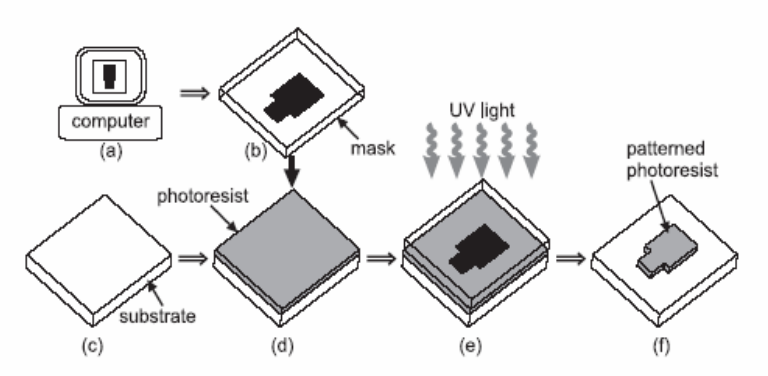

Figure 2-10. Photolithography process schematic. Image reprinted with permission from the Annual Review of Biomedical Engineering, Vol. 1, 1999, www.annualreviews.org.

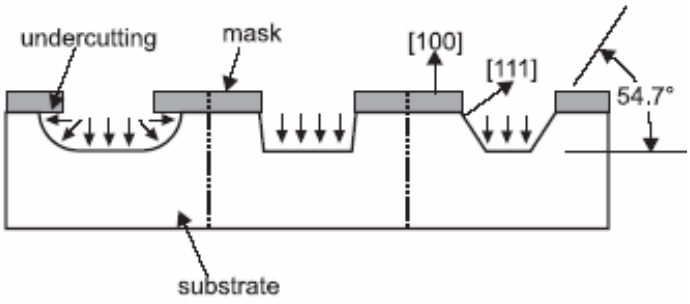

Figure 2-11. Schematic detailing silicon etch profiles. Left panel illustrates isotropic etching. Middle and right panels illustrate anisotropic etching. Image reprinted with permission from the Annual Review of Biomedical Engineering, Vol. 1, 1999, www.annualreviews.org.

CHAPTER 3
MATERIALS AND METHODS

Master Fabrication

The mask used for this project was manufactured by Pageworks (Cambridge, MA). The silicon masters were fabricated in Dr. Z. Hugh Fan's Microfluidics and BioMEMs laboratory, University of Florida. In brief, the silicon wafer was first cleaned and then primed with hexamethyldisilazane (HMDS). Next, AZ 1529 photoresist was spin coated onto the wafer and exposed to UV light. Subsequently, it was developed in AZ 312 MIF developer. Then, alternating deep reactive ion etching and passivation steps were repeated until the desired channel depth was reached. Next, the mask was shifted and the process was repeated to create a second depth within the channel[46, 47].

Cell Culture

Jurkat cells (a type of T-lymphocyte) were used during development and testing of the micro-scale migration device. Jurkat cells were obtained from Dr. Mark Segal in the Department of Medicine, University of Florida. The cells were cultured in a 37 ºC and 5% CO_2 environment in RPMI-1640 supplemented with 10% fetal bovine serum (FBS) (Fisher Scientific, USA).

Cell Counting

Cell density was enumerated using a SPotlite® hemacytometer (Baxter, USA). First, 10 μL of cell suspension were loaded into the hemacytometer by capillary action. Next, the cells were counted with a National DC3-163 digital microscope (National Optical & Scientific Instruments, San Antonio, TX).

Micropipette Experiments

Micropipettes were made by pulling glass capillary tubes (1.0 mm x 0.5 mm) to a fine point with a Narishige model PB-7 pipette puller (Narishige Company, Ltd., Tokyo, Japan) and

broken by quick fracture to the desired diameter. Pipettes were filled with a saline solution and flushed with bovine albumin (Fisher Scientific, USA) to prevent cell adhesion. The pipette was connected to two coupled fluid reservoirs for hydrostatic pressure control. Cells were suspended in PBS and loaded into a cell chamber that was held in a stage on an Axiovert 100 inverted light microscope (Carl Zeiss, Inc.). The proximal end of the micropipette was inserted into the cell chamber and cells were aspirated at a pressure of 5 cm H_20. Images were recorded with an external video system and Pinnacle Studio v.10.6 (Pinnacle Systems, USA) was used for image analysis.

Boyden Chamber Experiments

Disposable Boyden chambers with polyester membranes containing pores 8 μm in diameter (Corning, USA) were used for this project. For each experiment the membrane was soaked in RPMI 1640 media containing 10% FBS for 30 minutes, followed by 10 minutes of drying time. While the membrane was drying, the bottom wells of the 96-well plate were filled (245 μl in each) with chemoattractant concentrations ranging between 0.1 and 100 nM SDF-1. After filling the bottom wells the membrane was fitted into the well plate. Next, Jurkat cells were centrifuged at 250 *g* for 10 minutes in a Marathon 6K centrifuge (Fisher Scientific, USA). The supernatant was drawn off and the cells were rinsed in 1 mL of Hanks' Balanced Salt Solution 1X (HBSS) (Sigma Aldrich, USA). Subsequently, the cells were centrifuged again at 250 *g* for 10 minutes, followed by removal of the supernatant. The Jurkat cells were then resuspended in serum-free media (SFM) to a concentration of 6×10^5 cells/mL and 50 μl of the cell suspension was added to each top well. Therefore, a total of 3×10^4 cells were added to each top well. The chamber was then incubated at 37 °C in 5% CO_2 for 4 hours.

In addition to the range of SDF-1 concentrations, some bottom wells were filled with SFM to serve as negative controls. Chemokinesis controls were also done to measure the amount of random migration. These were done by suspending the cells in the upper wells in SDF-1 solution instead of SFM. The concentration of SDF-1 in the upper well equaled the concentration in the lower well, therefore, no gradient formed across the membrane.

After 4 hours of incubation, the solutions in the upper wells were discarded and the membrane was removed. The fluid in the lower wells was suctioned out, centrifuged, and resuspended in phosphate buffered saline. Subsequently, the number of cells in each sample was counted with a SPotlite® hemacytometer (Baxter, USA).

Statistical Analysis

Statistical analysis was performed with Microsoft Excel. A single-factor ANOVA test was used to determine significance between data sets. P-values less than 0.05 were considered statistically significant.

CHAPTER 4
RESULTS AND DISCUSSION

Specific Aim 1: Design a Microfluidic Device That Can Be Used to Induce Cell Deformation and Analyze Cell Migration

Micro-Device Design

The cellular migration device was designed to decrease reagent volumes, generate a chemical gradient via diffusion, and induce cell deformation. In addition, it was designed to allow for real-time analysis of migration, as well as provide a means of endpoint quantification of migration. The steps taken to realize the design are described below.

Device layout

Each migration device consists of two open wells connected by a single straight channel, as shown in Figure 4-1A. The CA well holds the chemoattractant, while the cell well holds the cell suspension. After loading the chemoattractant and cells, the chemoattractant begins diffusing through the channel toward the cell well. Once the cells sense the chemical they begin to migrate up the gradient, through the channel toward the CA well.

The migration device was designed so that there is no fluid flow within the device. This is critical given that flow biases cell migration. In the absence of fluid flow, diffusion is the only means of transport for the chemoattractant. As a result, migration is achieved solely through chemotaxis and/or chemokinesis.

The CA and cell wells were designed to act as an infinite source and sink, respectively. This was done by making the wells large enough to hold more than 6,000 times as much fluid as the microchannel holds. This allows the chemoattractant gradient to be maintained for more than 1 week.

Preliminary experiments were done in devices with a 1 mm long microchannel connecting the cell and CA wells. In these experiments the cells never migrated into the channel. This can

be explained by examining the gradient that forms within the device. Because the cell well acts as an infinite sink, the chemoattractant concentration drops to a negligible level at the point where the microchannel opens into the cell well (see Figure 4-2). Consequently, the concentration sensed by the cells is not strong enough to induce migration into the channel. In order to circumvent this problem, a cell holding chamber (CHC) was incorporated into the device between the microchannel and the cell well. The height of the CHC is greater than the height of the channel but significantly smaller than the height of the wells. The placement and dimensions of the CHC allow it to serve two purposes. First, it acts as a collection site for the cells and focuses their entry into the microchannel (see Figure 4-3). Secondly, it maintains the chemoattractant gradient, thereby placing the cells within an area of higher concentration (Figure 4-4). For instance, at the 4 hour time point the normalized concentration at the channel entrance in the device without a CHC is approximately 0.03 (Figure 4-2), while it is approximately 0.42 in the device with the CHC (Figure 4-4).

Dimensions

The migration device dimensions were chosen to maximize migration performance while minimizing assay cost. A complete list of dimensions for the device is given in Table 4-1. The rationale employed for setting these dimensions is described below.

Chemoattractant (CA) and cell wells. The width of the wells was chosen so that fluid could easily be loaded into the wells using a commercially available pipetter. This dictated a minimum well diameter of 3 mm. Due to availability, a 3.5 mm diameter punch was used to create the wells.

The height of the wells is a function of how much polymer is used to fabricate each device. It is economically advantageous to minimize the volume of materials used. However, there is a minimum thickness of polymer required to prevent the channel from collapsing during the

vacuum filling procedure (described in Specific Aim 2). If the polymer layer on top of the microchannel is too thin, the negative pressure created by the vacuum pulls the roof of the microchannel down and seals it to the floor of the channel. The minimum well height found to prevent channel collapse is 2.5 mm.

With a well diameter of 3.5 mm and a height of 2.5 mm, the total volume of each well is approximately 24 μL. Filling the wells to the top made it difficult to cover and seal the wells. To allow for airspace in the wells, 20 μL of chemoattractant and cell suspension were loaded into the CA and cell wells, respectively, for each migration assay. This volume of chemoattractant is more than 10 times less than the volume required for some Boyden chamber migration assay (~245 μL).

Microchannel. The height of the microchannel is the feature that forces cells to deform in order to migrate through the device. Therefore, the height must be smaller than the diameter of the cells being tested with the device. Jurkat cells have an average diameter of 13.2 ± 1.7 μm (Appendix A). Low-pressure (5 cm H_2O) micropipette aspiration experiments were performed to determine the ability of Jurkat cells to deform and enter pipettes with inner diameters of 6, 8, and 10 μm. The tests showed that Jurkat cells cannot fully deform to pass through a 6 μm constriction. Conversely, 8 μm is big enough for the cells to deform through (75% of cells fully entered the pipette). Furthermore, 100% of the cells tested with the 10 μm pipette were fully aspirated. Based on this data, the preliminary microchannel height was chosen to be 8 to 10 μm. Prototype devices were manufactured with microchannel heights of 8 and 10 μm and the experimental results obtained from each were compared to choose the final channel height. As later described in Specific Aim 3, 10 μm was chosen as the final channel height for testing Jurkat cells in the micro-scale migration device.

The length of the microchannel was chosen based on the shortest length that could reproducibly be fabricated. The shorter the channel length, the shorter the distance the cells must migrate to reach the CA well. More cells can traverse a shorter channel than they can a longer channel in the same period of time. This maximizes the number of cells that are counted at the end of the assay. Additionally, the shorter the channel, the steeper the concentration gradient. Cell migration rates are known to increase as gradient steepness is increased[48]. The channel length varied slightly between test devices because the wells for each device were punched by hand. The shortest length that could be produced was approximately 100 μm.

A width of 500 μm was chosen for the channel. This width was large enough to allow multiple cells to migrate, side-by-side through the channel. This increases throughput and minimizes channel clogging. If a rigid cell gets lodged in the channel other cells can continue migrating by moving around the blockage.

Cell holding chamber (CHC). As previously mentioned, the CHC serves two purposes: to collect and line up cells along the microchannel entrance, and to maintain a steep chemical gradient. In order to facilitate cell positioning within the CHC, the height of the CHC must be larger than the size of the cells. To maintain a steep gradient the height must be close to the height of the microchannel. To satisfy both of these requirements, the CHC height was chosen to be ~20 μm. Due to ease in the master fabrication process, the CHC height was fixed as 24 μm.

The length of the CHC affects the gradient within the microchannel. Diffusion within the device is described by Fick's 2nd Law of diffusion:

$$\frac{\partial c}{\partial t} = D\nabla^2 c \qquad \text{Equation 4-1}$$

where *c* is concentration (mass/vol or mols/vol) and D is the diffusion coefficient (length^2/time). Comsol Multiphysics v. 3.5 software was used to model diffusion within the migration device

(Appendix B). Figure 4-5 illustrates the effect of CHC length on the gradient. When the CHC length is increased, the chemoattractant concentration at the channel entrance increases. For example, the normalized channel inlet concentration for a 200 μm CHC is approximately 0.52 while that for a 500 μm CHC is approximately 0.7. This is beneficial because it decreases the required concentration of chemoattractant loaded into the CA well, which decreases the cost of each assay. Based on this, the CHC should be relatively long compared to the length of the microchannel. However, the longer the CHC is, the more time it takes to position the cells. As a result, the CHC length was set as 200 μm. This gives a normalized chemoattractant concentration of 0.52 at the channel entrance while allowing cell positioning to be performed in a reasonable amount of time (~30 min).

The channel and CHC were etched to different depths (~10 μm and 24 μm, respectively) using a single photomask. This was done by shifting the mask and performing two separate etch cycles. This made it necessary for the CHC to be an extension of the microchannel. Therefore, its width is equal to that of the microchannel (500 μm).

In summary, the following dimensions were chosen for the CHC: height, 24 μm; length, 200 μm; and width, 500 μm. With these dimensions the volume of the CHC is 2.4×10^{-3} μL. Adding this to the volume of the microchannel (5×10^{-4} μL) gives a total of 2.9×10^{-3} μL in which the gradient is maintained. The volume of fluid in each well is nearly 7000 times greater than that of the CHC and microchannel combined, thereby creating an infinite source and sink. This is illustrated graphically in Figure 4-6. This simulation shows that a gradient can be maintained for more than 1 week.

Micro-Device Fabrication

The device layout and corresponding dimensions were incorporated into a silicon master via photolithography by the personnel in Dr. Z. Hugh Fan's Microfluidics and BioMEMs laboratory (University of Florida). This process is outlined in the Materials and Methods section of this paper. The silicon master was used to imprint the microchannel design into a soft polymer. Subsequently, the polymer was bonded to a glass slide to create the enclosed microchannel. The steps taken to develop the fabrication protocol are detailed below.

Casting and punching

The material used for fabricating the devices must be transparent, non-toxic, easy to fabricate, and strong enough to withstand vacuum suction during channel filling. Microfluidic devices are commonly cast out of poly(dimetheylsiloxane) (PDMS) because it is economical, non-toxic, easy to use, and transparent. There are several PDMS elastomers available, with varying properties. Two different PDMS elastomers were used for this project, Slygard® 184 (S-184) and Silastic® T-2 RTV (T-2) (Dow Corning, USA). In its uncured state, S-184 is less viscous than T-2 (3.9 Pa·s and 55 Pa·s, respectively[49]). As a result, S-184 is easier to mix and pour, it self-levels quickly, and it takes less time to de-gas than T-2. While these features made it easy to fabricate devices with S-184, they were not stiff enough to withstand the vacuum suction used during channel filling. In its cured state T-2 is stiffer than S-184 (E = 5.5 MPa and 2.6 MPa, respectively[49, 50]), and can thus withstand the suction without collapsing the channel structure. To satisfy both material requirements the two PDMS elastomers were mixed. The ratio of the two elastomers was varied to find the minimum amount of T-2 required to prevent channel collapse. Ratios of 9:1 and 8:2 (S-184:T-2) did not prevent channel collapse. However, a 7:3 ratio of S-184 to T-2 made the devices stiff enough to prevent collapse.

The S-184 and T-2 were each prepared by mixing a 10:1 (v/v) ratio of base to curing agent, respective to each polymer. The two elastomers were then mixed together in a 7:3 ratio (S-184 to T-2). The mixture was degassed in a vacuum chamber for 20 min and subsequently poured onto the silicon master. Any bubbles that remained were popped by blowing CO_2 across the surface. The S-184/T-2 was cured in a 250° F oven for 1 hr and then peeled off the silicon master. A 3.5 mm biopsy punch (Miltex, York, PA) was used to punch the wells on both ends of the microchannel.

Cleaning and bonding

Many of the microfluidic devices reported in the literature are fabricated by bonding PDMS to glass slides via oxygen plasma treatment. This process creates a strong, irreversible bond. The patterned S-184/T-2 pieces were treated with oxygen plasma and then manually pressed onto glass slides. During this process the channel collapsed and the roof of the microchannel was irreversibly bonded to the glass slide, effectively sealing the channel. Due to its small height (10 μm) the channel could not withstand the pressure required to bond the materials with this method. As a result, an alternative method was established.

PDMS adheres to glass if both materials are exceptionally clean. The patterned S-184/T-2 pieces were cleaned by sonication in a solution of Sparkleen detergent (Fisher Scientific, USA) and deionized (DI) water for 5 min. Next, the pieces were rinsed by sonicating them in fresh DI water for 5 min, a total of 3 times. After rinsing, the pieces were dried with N_2 gas. Glass slides were cleaned by soaking them in 1 M hydrochloric acid for 1 min. Next, they were rinsed by dipping them in DI water followed by 70% ethanol. Finally, they were dried with N_2 gas. The clean PDMS pieces were bonded to the clean slides by contacting the two surfaces and tapping around the channels. The assembled devices were placed in a 37° C environment overnight. The

resulting bond between the PDMS and glass was strong enough to withstand manipulation throughout the course of the migration assay.

Due to the short duration of these assays (4 hr), it was not necessary to sterilize the devices. However, migration studies carried out over several days must be done under sterile conditions. The micro-devices can be autoclaved for use in longer assays.

Specific Aim 2: Develop the Migration Assay Protocol

The micro-device migration experiments were first set up by filling the channels with SFM, preparing and positioning the cells, and loading the chemoattractant. Once the devices were set up cell migration was observed via video recordings. After the allotted assay time the migrated cells were fixed and stained to achieve an endpoint quantification of chemotaxis.

Channel Filling

Several methods were tried for filling the microchannels with media. With many microfluidic devices the channels can be filled by loading fluid into one well and then letting capillary action draw the fluid through the channel. This method was unsuccessful in the micro-scale migration devices because the resistance to fluid flow into such a small channel was too great. Another common method involves forcing fluid through the channel via syringe. The force exerted in this method disrupted the bond between the PDMS and the glass slide, thereby destroying the migration devices. A third method that is commonly employed is done by filling one well with fluid and pulling it through the channel via suction from a vacuum hose attached to the opposite well. This method resulted in collapsing the microchannel before any fluid could be drawn through it. Finally, an alternate vacuum filling method was found to successfully fill the microchannels. This technique is detailed below.

Assembled micro-devices were fitted with a media reservoir as illustrated in Figure 4-7. SFM was pipetted into the reservoir until the device was completely submerged with

approximately 2 mm of media on top of the device wells. The media reservoir served to keep the wells submerged with fluid while minimizing the volume of fluid required (250 μL). The device was then placed inside a vacuum chamber and the vacuum was applied for 20 minutes. After turning off the vacuum pump, the vacuum chamber remained closed for 1 min. to return to atmospheric pressure. Next, the device was removed from the chamber and the media was removed from the reservoir[51]. The channels were inspected via microscopy to make sure they were filled and free of bubbles. For demonstrative purposes, several channels were filled with fluorescent dye (see Figure 4-8). This clearly shows that the channels are completely filled using this method.

Cell Preparation

Jurkat cells were centrifuged at 250 *g* for 10 minutes in a Marathon 6K centrifuge (Fisher Scientific, USA). Subsequently, the supernatant was drawn off and the cells were rinsed by resuspending the pellet in 1 mL of Hanks' Balanced Salt Solution 1X (HBSS) (Sigma Aldrich, USA). Next, the cells were centrifuged again at 250 *g* for 10 minutes, followed by removal of the supernatant. The cells were resuspended in 1 mL of SFM then counted using a SPotlite® hemacytometer (Baxter, USA). After counting, the cells were diluted to a concentration of 3 x 10^6 cells/mL of SFM.

Cell Positioning and Chemoattractant Loading

After filling the micro-channel with media the wells were emptied by gently removing the media with a pipette. Next, 20 μL of cell suspension was added to the cell well. No fluid flow resulted from this addition because the force exerted on the fluid open to the CA well exceeded the force exerted by the fluid in the cell well (5.07 x 10^{-4} N and 2.35 x 10^{-7} N, respectively—see Appendix C for calculations). Therefore, the cells remained in the cell well during this step.

Next, 20 μL of SDF-1 was added to the CA well and both wells were quickly covered with a piece of transparent tape. The tape was necessary to prevent pressure-driven flow in the device. The flow rate within a microchannel is calculated using the formula

$$Q = \frac{\Delta P}{R} \qquad \text{Equation 4-2}$$

where Q is the volumetric flow rate, ΔP is the pressure drop across the channel, and R is the resistance. The pressure drop can be calculated using the formula

$$\Delta P = \rho g \Delta h \qquad \text{Equation 4-3}$$

where ρ is the density of the fluid, g is the acceleration due to gravity, and Δh is the change in height of the fluid levels on either side of the channel. For a rectangular microchannel with h << w, the resistance is given by

$$R = \frac{12 \mu L}{w h^3} \qquad \text{Equation 4-4}$$

where μ is the fluid viscosity, L is the channel length, w is the channel width, and h is the channel height[52]. Ideally, the fluid heights in each well would be equal, thereby eliminating a pressure drop across the channel. This would prevent flow (see Equations 4-2 and 4-3). However, it is very difficult to obtain equal fluid heights when using micro-scale volumes. As a result, flow is inevitable (See Appendix C). Sealing the wells with tape closes the system so that fluid is not displaced in either well.

Once the device was sealed it was tilted at a 90° angle, with the cell well elevated above the CA well. Tilting the device allowed gravity to pull the cells into the CHC so that they lined up along the channel entrance (Figure 4-9). Each device was checked via microscopy to make sure cells had entered the CHC. The time it took to position the cells varied because the length

of the CHC varied between devices (because the wells were punched by hand). However, cells could be positioned in most of the devices within ~30 min. The final version of the device will be manufactured to have uniform channel and CHC lengths. As a result, the cell positioning time will be standardized.

Endpoint Quantification of Migration

After 4 hrs the fluid within the CA well was gently removed and replaced with 100% methanol to fix the cells to the glass slides that comprised the bottom of the device. After 15 minutes the methanol was removed and replaced with Harris Modified hematoxylin (Sigma-Aldrich, USA) to stain the cells for 5 minutes. After staining, the hematoxylin was removed and the wells were rinsed with DI water until the water ran clear. The stained cells were clearly visible (as shown in Figure 4-10) and easy to count. This method is advantageous because it does not require any specialized equipment or expertise. The cell count in the CA well is plugged into Equation 4-5 to calculate the migration ratio (MR_{micro}).

$$MR_{micro} = \frac{\#\,StainedCells}{\#\,LoadedCells} \qquad \text{Equation 4-5}$$

MR_{micro} is defined as the ratio of stained cells (in the CA well at t = 4 hr) to the number of cells loaded into the cell well at t = 0.

Specific Aim 3: Test the Microfluidic Migration Device

Gradient Visualization

The generation and maintenance of the gradient within the micro-scale migration device was visualized with the fluorescent dye fluorescein isothiocyanate (FITC). Dextran tagged with FITC was used. FITC-dextran can be purchased in a wide range of molecular weights (MW). The MW of SDF-1 is ~10 kDA (R & D Systems), therefore, 10 kDa FITC-dextran was used to approximate the gradient formed by SDF-1. The diffusion coefficient for FITC-dextran[53] (D_{FITC-}

$_{Dextran,\ 10\ kDa}$ = 1.7 x 10^{-6} cm^2/s) was used in the Comsol Multiphysics simulation so that it could be compared to the experimental results. To demonstrate the gradient, a device with the following dimensions was used: channel (height = 10 μm, length = 400 μm, width = 500 μm), CHC (height = 24 μm, length = 550 μm, width = 500 μm). A longer channel and CHC were used for the demonstration because shorter channels were obscured by a fluorescent bloom that resulted from fluorescence saturation in the two wells. The channel, CHC, and cell well were loaded with phosphate buffered saline (PBS), while the CA well was loaded with a 1 mM solution of FITC-dextran. As the gradient formed over time, images were taken with an Axioplan 2 imaging microscope with an attached AxioCam HRc camera (Zeiss) (see Figure 4-11). The fluorescence intensity was measured using Adobe Photoshop CS3 (version 10.0). The fluorescence intensity within the channel and CHC was normalized to the intensity in the CA well (so that it could be compared to the normalized simulation values). Since the CHC is 2.4 times taller than the channel, the larger volume of fluid in the CHC produced a skewed intensity. To correct this, the measured intensity in the CHC was divided by 2.4. This made it possible to continue tracking the gradient through the CHC. The experimental and theoretical results are given in Figure 4-12A and Figure 4-12B, respectively. A fluorescent gradient could be measured within 5 minutes. The fluorescent intensity within the channel continued to increase until ~ 1 hr after loading, at which point it stabilized for 1 day. This agrees with the theoretical results (the 1, 4, and 24 hr plots are very close together, see Figure 4-12B. After 1 day, the intensity gradually increased and at day 7 it reached a normalized intensity of ~0.19 at the channel entrance. The presence of a gradient for 7 days or more shows that the microfluidic device can be used for long-term migration assays.

It is evident from the plots A and B in Figure 4-12 that all the experimental values are lower than the theoretical values. This is most likely due to limitations in the experimental analysis method. The fluorescent intensity was measured in terms of pixels with Adobe Photoshop CS3 (v. 10.0). The large volume of fluorescent dye in the CA well saturated the image (maximum pixel count = 255 pixels), skewing the true intensity for that well. Because the channel and CHC intensities were normalized with respect to the CA well, all values were lowered. Despite the difference in measured values, the rate at which the experimental gradient formed, stabilized, and began to decay were similar to the theoretical results. To correct the skewed values, random experimental data points were compared to the theoretical results to determine the appropriate CA well intensity (43 pixels for the 5 min data and 108 pixels for all other time sets). Based on these values, all data points were scaled, as shown in Figure 4-12C. This more closely mimics the theoretical simulation. In fact, the scaled intensities at the channel inlet are very similar to the theoretical concentrations (e.g. scaled intensities for 1 hr = 0.34 and 7 days = 0.45 as compared to the theoretical values of 1 hr = 0.38 and 7 days = 0.49). The similarity between the experimental results and the theoretical approximation in this case indicates that theoretical calculations can confidently be used to assess the effects of varying the device dimensions (see Appendix D).

Observed Deformation and Migration

Cell deformation is fundamental to the design of the micro-scale migration device. The channel height was chosen to force the cells to deform in order to migrate through the device. The average measured diameter of the Jurkat cells in the 10 μm tall channel was approximately 2.5 μm larger than the un-deformed cells in the CHC (cells in channel: 15.7 ± 1.5 μm (n=30),

cells in CHC: 13.2 ± 1.7 μm (n=30) Appendix A) proving that the cells within the channel are deformed.

PDMS is transparent; therefore cell migration through the device can be observed via microscopy and/or cell tracking software. A Zeiss Axiovert 100 inverted light microscope (Carl Zeiss Inc., Germany) was used to monitor migration within the micro-scale device. Figure 4-13 illustrates cells migrating through the device. As the assay progressed cells migrated through the channel and collected in the CA well. The average measured migration of the Jurkat cells through this channel was 66 ± 20 μm/hr (channel height = 10 μm, SDF-1 concentration = 100 nM).

Migration Quantification Method

The "experimental" method used to quantify migration differed from the "ideal" method described previously in Specific Aim 2. In brief, the "ideal" method involves staining and counting cells that migrate through a 100 μm channel and into the CA well. This method had to be altered for use with the prototype devices since the channel length varied because the wells were punched by hand. Most of the channels were longer than 100 μm. As a result, many cells migrated 100 μm or more but did not travel into the CA well because the channel was too long. Hence, if the quantification method for the "ideal" device were used for the prototypes, many cells that had migrated 100 μm or more would not be stained and counted because they hadn't yet entered the CA well. This would produce variability in the results obtained. To combat this, the "experimental" method counted cells in the CA well and also within the channel. This is illustrated in Figure 4-14, in which the device has been divided into cell counting zones. Equation 4-6 was used to calculate the migration ratio for the micro-devices (MR_{exp}).

$$MR_{\exp} = \frac{(C_4 + D_4) - (B_0 + C_0 + D_0)}{A_0} \qquad \text{Equation 4-6}$$

MR_{exp} is defined as the ratio of the total number of cells that deformed, entered, and migrated (100 μm or more) to the total number of cells positioned within the CHC at the start of the assay. As illustrated in Figure 4-14, zone A denotes the CHC, zone B is the first 100 μm of the channel, zone C is the remainder of the channel, and zone D is the CA well. Any cells that were forced into the channel during the cell positioning step (a result of varying CHC length) were subtracted from the number of cells present in zones C and D at t = 4 hr so that only cells that started in the CHC (un-deformed) would be counted as "migrated cells." The total number of cells that migrated (the numerator in Equation 4-6) must be less than the number of positioned cells (denominator in Equation 4-6). If the amount of migrated cells exceeds the amount of positioned cells it shows that additional cells from the cell well entered and migrated through zones A and B during the assay. If this occurs the assay time should be decreased so that any cells that enter zone A during the assay will not migrate into zone C.

Zone A was limited to 200 μm because the "ideal" CHC length was set as 200 μm (as described in Specific Aim 1). Due to variations in CHC length within the prototype devices (again due to punching the wells by hand) the number of cells positioned within each CHC varied. This is a function of how quickly the cells can be positioned. In longer CHCs, cells must travel farther to enter zone A. Thus, given the same amount of time, more cells can be positioned within zone A of a shorter CHC than in a longer CHC. To account for this variability, migration was normalized by dividing the number of migrated cells within each device to the number of cells positioned within that device at t = 0.

It should be noted that the final version of the device will have consistent channel and CHC lengths (100 μm and 200 μm, respectively). As a result, the "ideal" method for quantifying migration, including Equation 4-5 should be used. This will significantly reduce analysis time.

Preliminary data

Preliminary migration experiments were performed with Boyden chambers (pore size = 8 μm) to determine the SDF-1 concentration range that would be used to test the micro-scale migration devices. The migration ratio for the Boyden chambers (MR_{Boyden}) was calculated using Equation 4-7.

$$MR_{Boyden} = \frac{\#\,MigratedCells}{\#\,LoadedCells} \qquad \text{Equation 4-7}$$

The MR_{Boyden} is defined as the number of cells that migrated through the filter divided by the number of cells loaded into the top well at the start of the assay. The results for the Boyden chamber migrations are given in Figure 4-15. The top of the range was set as 100 nM SDF-1 because this was the highest concentration that was economically feasible to use. The MR_{Boyden} increased proportionally with the increase in SDF-1 from 0.1 to 100 nM concentrations. The ratio for 0.1 nM SDF-1 did not differ statistically from the ratio for the negative control (0 nM SDF-1), therefore, the testing concentrations were set as 1, 10, and 100 nM.

Quantification of Jurkat cell migration

Micro-scale migration devices with a channel height of 10 μm were used to quantify Jurkat cell migration in the presence of 1, 10, and 100 nM SDF-1. The results are given in Figure 4-16. The data trend shows a direct relationship between migration ratio and SDF-1 concentration. This effect was expected as cells have been shown to migrate faster in the presence of higher chemoattractant concentrations. The migration ratio for 1 nM SDF-1 differed significantly from that for the negative control (0 nM SDF-1) ($p = 0.016$) and for 10 nM SDF-1 ($p = 0.002$).

However, the migration ratios for 10 nM and 100 nM SDF-1 did not differ statistically ($p = 0.187$). The standard deviation within each data set can be attributed to variations in channel and CHC lengths (a result of hand-punching). As described in Specific Aim 1, the length of the channel and the CHC affect the steepness of the gradient. As a result, cells will migrate at different rates through channels of different lengths. This was demonstrated experimentally, as illustrated in Figure 4-17. As the channel length was increased the migration ratio decreased. To reduce the variability caused by increasing channel length the data included in Figure 4-16 was taken from devices with channel lengths of 400 μm or less. This provided enough data points to demonstrate the trend while also minimizing the standard deviation within each set.

Quantifying migration is advantageous because it allows comparisons to be made between the migratory ability of various cell samples. For instance, migration assays can be utilized to test the efficacy of drugs intended for the treatment of rigid, diseased cells. Treated and untreated samples can be tested with the micro-scale migration device, and the migration ratios can be compared to determine how effective the drug is in improving cellular deformation and migration. Comparisons can be made as long as experimental parameters (e.g. chemoattractant concentration, device dimensions, assay time) are kept constant between samples.

Chemokinesis

Separating the effects of chemotaxis (directed migration) and chemokinesis (random migration) is essential for studying cellular migration in the body. For instance, leukocytes migrate to areas of injury and infection within the body. The leukocytes crowd together inside capillaries prior to migrating through the capillary walls and into the surrounding tissue. The dense packing of the leukocytes induces the secretion of neutrophil cytosol, a chemokinetic agent. This stimulates random migration, which enables the leukocytes to penetrate further into

and through the vessel wall and surrounding tissue where the chemotactic gradient is strong enough to attract the cells to the site of injury[54]. In this case, both chemokinesis and chemotaxis are used to facilitate cell migration through the body. Therefore, it is important to study both modes of migration.

Separating chemotaxis and chemokinesis using the Boyden chamber requires multiple experiments. Migration experiments were done as previously described: chemoattractant was loaded into the bottom well and cells were suspended in SFM in the top well. The migration measured in this test includes chemotaxis and chemokinesis. Therefore, it is referred to as a measure of "net migration." Experiments that measured chemokinesis only were performed by suspending the cells within the top well in the same chemoattractant concentration that was loaded into the bottom well. The chemokinesis count must be subtracted from the net migration count to get the chemotaxis count. Boyden chamber chemokinesis experiments were performed for this project. The results are shown in Figure 4-18. A statistical difference between quantified chemokinesis and net migration was only seen for the 100 nM case. This shows that an SDF-1 concentration greater than 10 nM is required to separate the effects of Jurkat cell chemotaxis and chemokinesis in the Boyden chamber. Consequently, this increases the assay cost.

Chemokinesis experiments were performed in the micro-scale migration device by filling the channels with SDF-1 as well as suspending the Jurkat cells within the cell well in SDF-1 instead of SFM. As a result, the SDF-1 concentration was uniform throughout the device. Chemokinesis tests were done with 100 nM (n=3) and 10 nM (n=3) SDF-1. Figure 4-19 shows a 100 nM SDF-1 chemokinesis experiment at t = 0 and t = 4 hr. It is evident that some of the cells migrated randomly (non-vectorial movement) as their positions within the channel are slightly

changed between the start and end of the assay. However, none of the cells migrated a net 100 μm through the channel toward the CA well. This was the case for all the chemokinesis tests performed with the micro-scale migration devices. This shows that the micro-scale device (with a channel length of 100 μm) quantifies Jurkat cell chemotaxis only (no chemokinesis).

The lack of measured chemokinesis in the micro-scale device is due to the channel length. 100 μm is too far for the cells to randomly migrate during the assay. This is not the case for the Boyden chamber. The filter within the Boyden chamber is approximately 10 μm thick. Therefore, the cells only have to migrate 10 μm to enter the lower well where they are counted. 10 μm is a short distance through which cells can randomly migrate in a net direction.

Even though chemokinesis is excluded from the measured migration in the micro-scale device, chemokinesis experiments can be conducted with this device. As previously described, the channel, cell well, and CA wells should all be filled with the same chemoattractant concentration. Cell chemokinesis would then be monitored in real-time via microscopy.

Effect of channel height on migration

The channel height within the micro-devices was altered to examine the effect deformation has on the number of cells that migrate through the device. Experiments were performed using channel heights of 8 μm and 14 μm. These results were compared to the results obtained from devices with 10 μm tall channels (see Figure 4-20).

It was expected that decreasing the channel height to 8 μm would decrease the measured migration ratio as fewer cells would be able to deform enough to migrate into and through the microchannel. The results show that this was the case. In fact, the average measured migration ratios for the 100, 10, and 1 nM SDF-1 tests were 0.006, 0.004, and 0, respectively (Figure 4-20). The majority of the cells could not deform enough to enter the channel. In one of the

experiments, some cells were forced into the channel during cell positioning. These cells did migrate through the channel, as illustrated in Figure 4-21. However, un-deformed cells in the CHC did not leave the CHC during the 4 hour assay. This proves that the concentration gradient was present and strong enough to make the cells migrate, but not strong enough to force the cells to deform. Based on this, it is concluded that an 8 μm channel height is too small to be used with Jurkat cells.

Jurkat cells are 13.2 ± 1.7 μm in diameter (Appendix A). Therefore, most Jurkat cells do not have to deform to migrate through a 14 μm tall channel. Consequently, increasing the channel height to 14 μm was expected to increase the measured Jurkat migration ratio. As illustrated in Figure 4-20, this did not happen. The migration ratios for 14 μm and 10 μm channel heights were not statistically different (when the same SDF-1 concentration was used). This suggests that Jurkat cells are deformable enough to quickly deform into a 10 μm channel. This confirms that 10 μm is the ideal channel height to be used for Jurkat cell migrations.

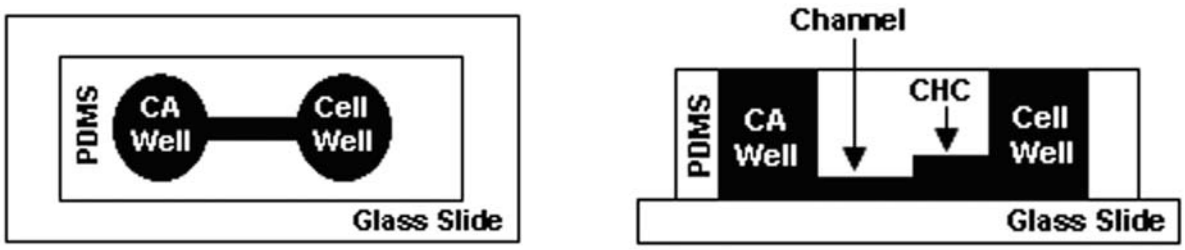

A B

Figure 4-1. Micro-scale migration device schematic; A) top view, B) side view. Images not drawn to scale. CA stands for chemoattractant. Areas shaded in black denote portions of device that contain fluid and cells.

Table 4-1. Microscale migration device dimensions.

Microscale device dimensions	
Wells:	
Diameter:	3.5 mm
Height:	2.5 mm
Channel:	
Length:	100 µm
Width:	500 µm
Height:	10 µm
CHC:	
Length:	200 µm
Width:	500 µm
Height:	24 µm

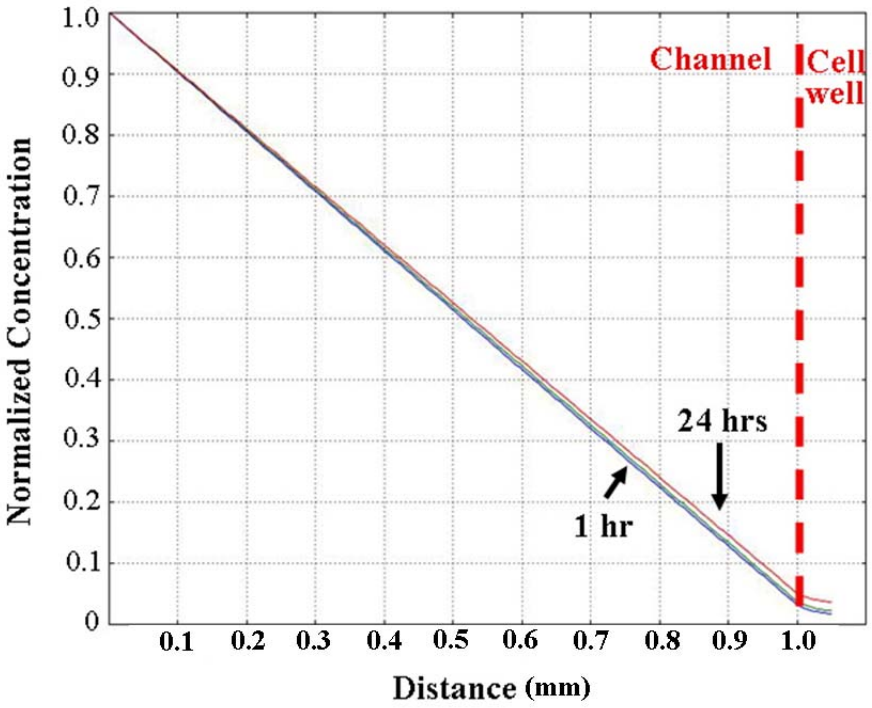

Figure 4-2. Simulated concentration gradient within a microchannel of uniform depth. The x-axis represents the distance from the CA well.

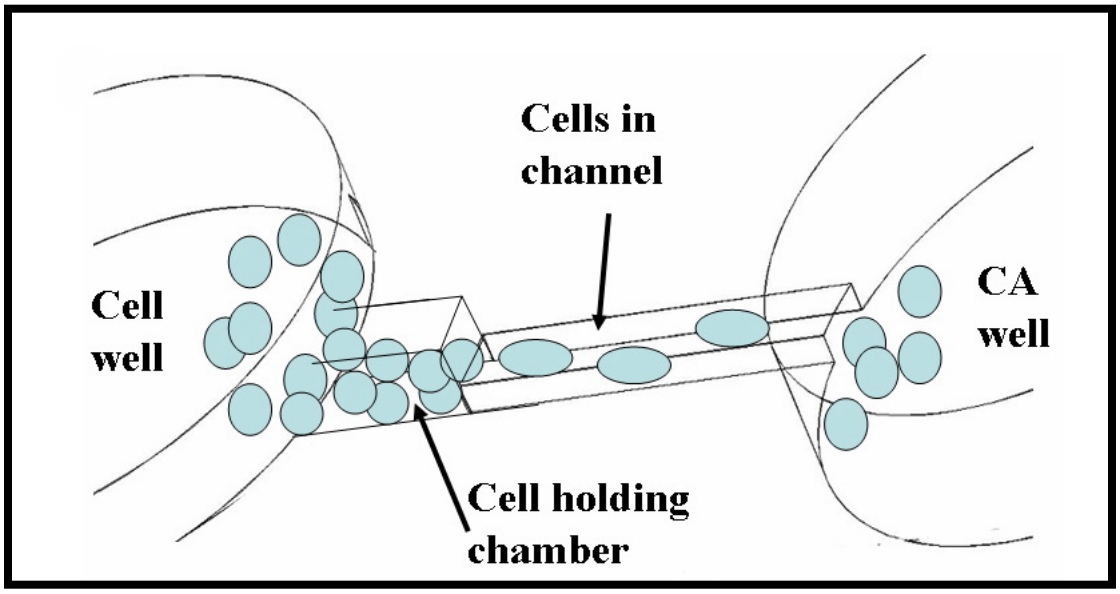

Figure 4-3. Schematic of micro-scale migration device with cell holding chamber (CHC). Cells are positioned within the CHC then they deform into the channel and migrate towards the CA well. Image not drawn to scale.

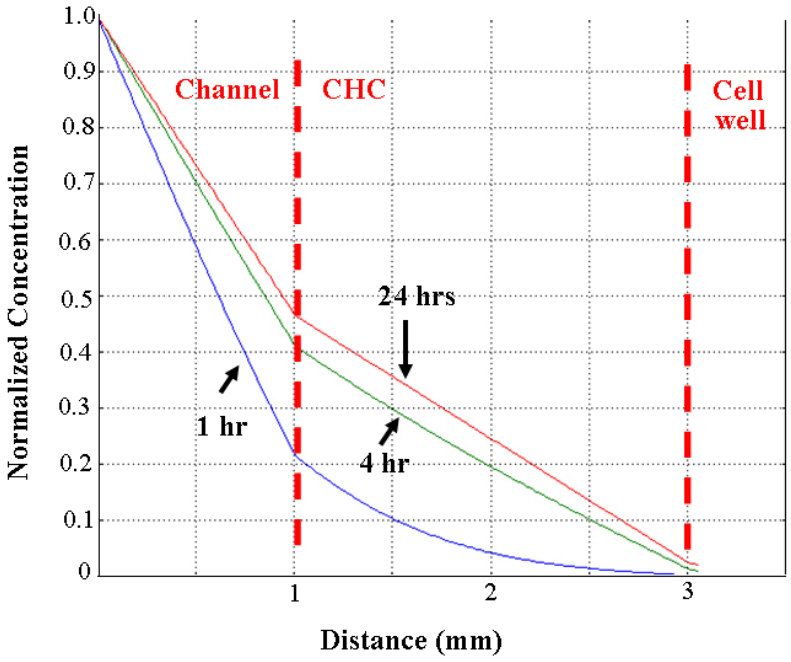

Figure 4-4. Simulated concentration gradient within a device with a CHC.

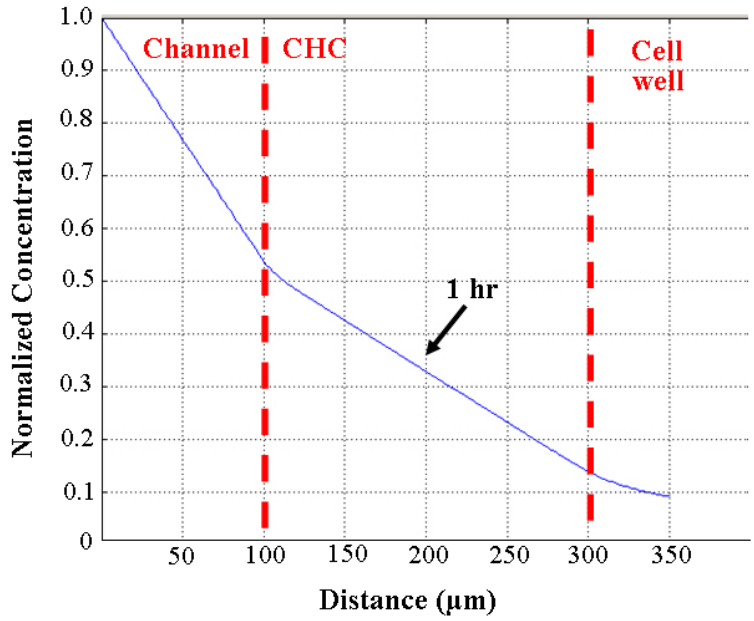

A

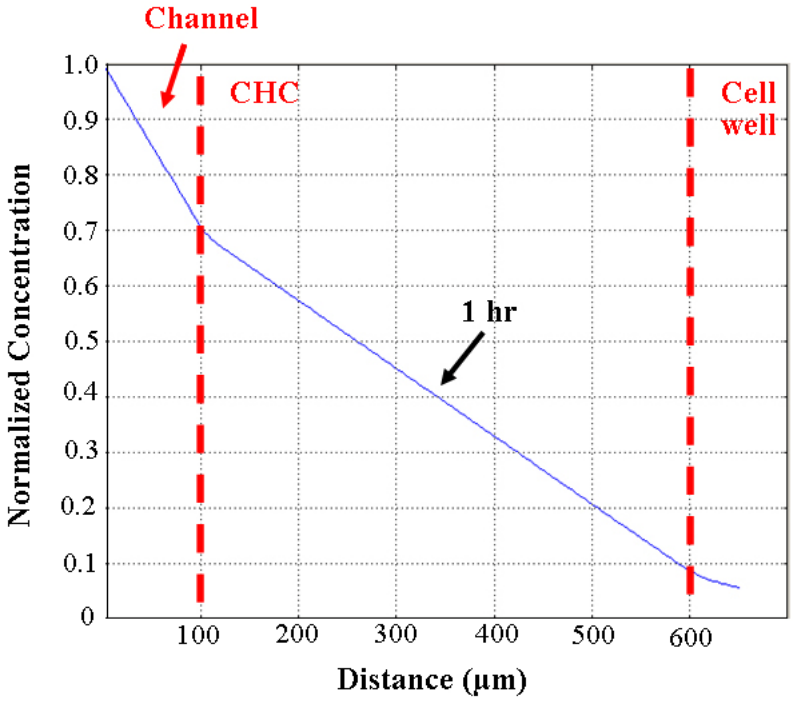

B

Figure 4-5. Effect of CHC length on gradient. Diffusion simulations for A) 200 µm and B) 500 µm length CHC. The channel height was set as 10 µm and the CHC height was set as 24 µm for both A) and B).

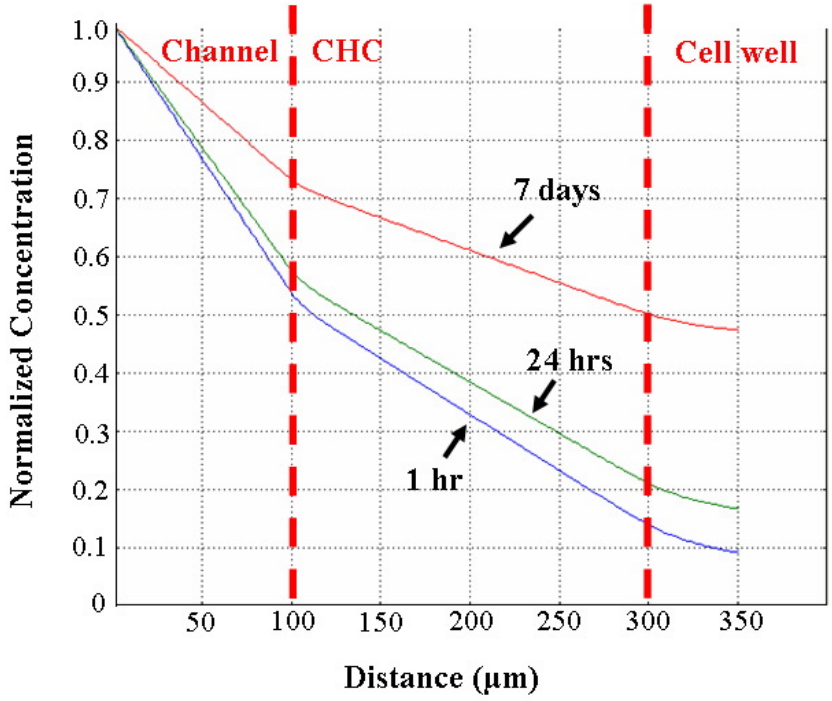

Figure 4-6. Diffusion simulation demonstrating presence of gradient up to 7 days.

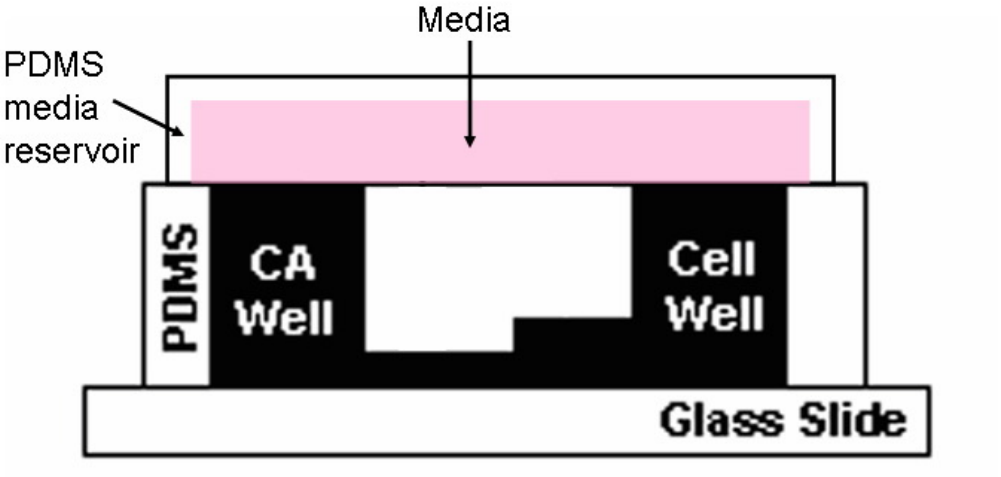

Figure 4-7. Schematic showing media reservoir fitted on top of micro-device.

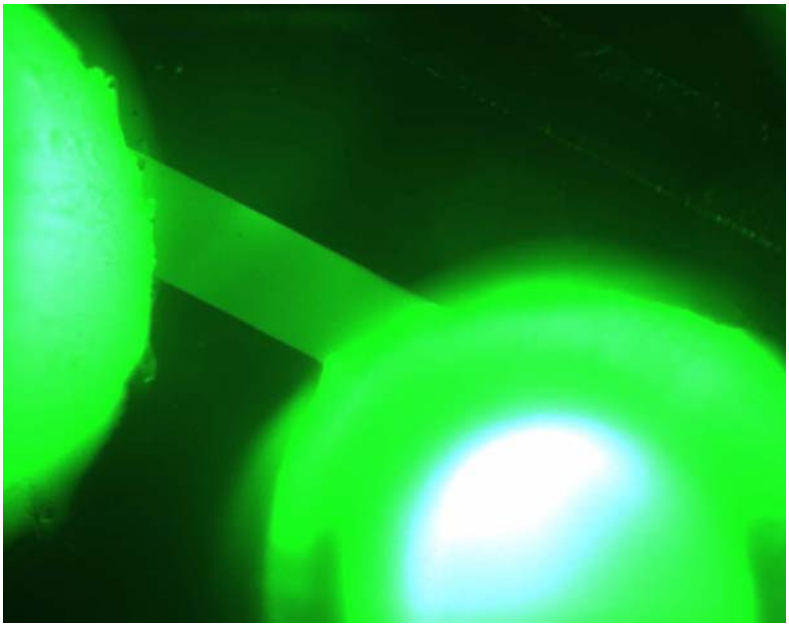

Figure 4-8. Microchannel filled with fluorescent dye.

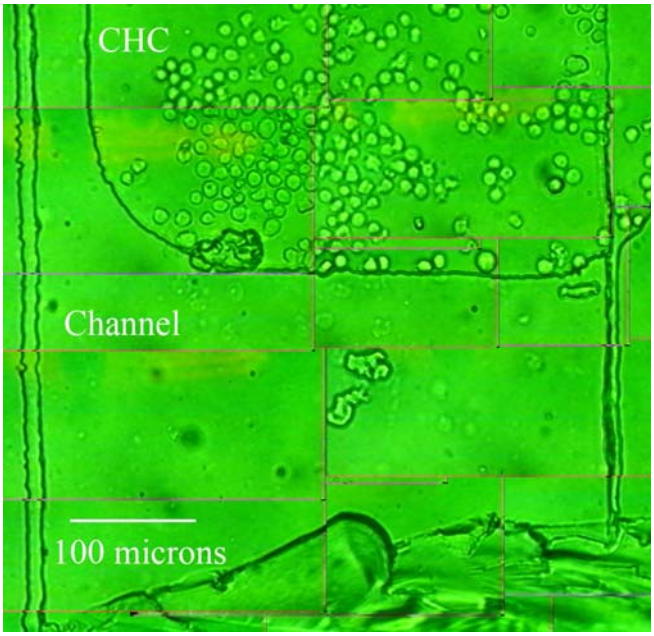

Figure 4-9. Jurkat cells positioned within CHC.

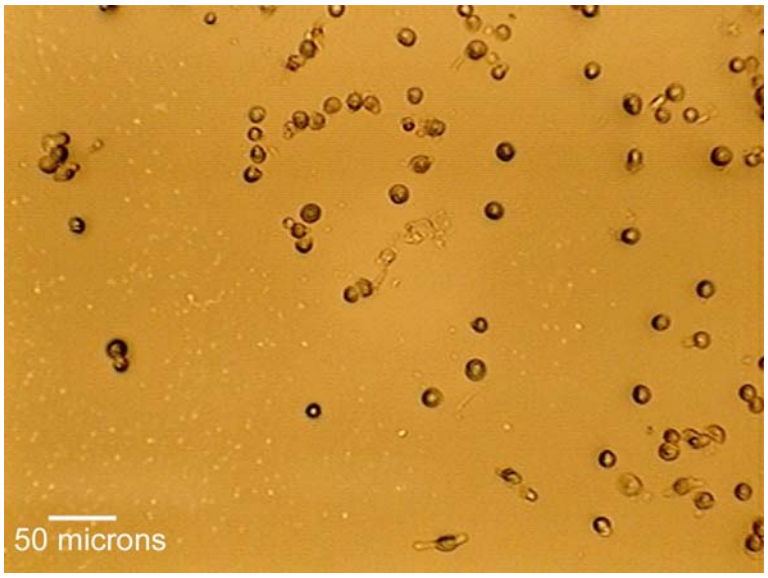

Figure 4-10. Jurkat cells stained within the chemoattractant (CA) well.

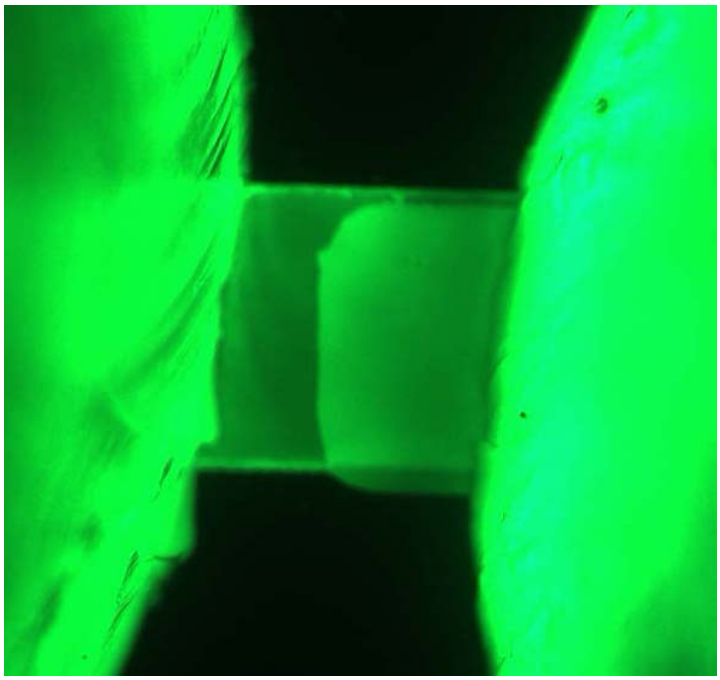

Figure 4-11. Fluorescein isothiocyanate (FITC)-dextran solution in the micro-device. The varying fluorescent intensity in the channel and CHC was measured to graph the gradient formation.

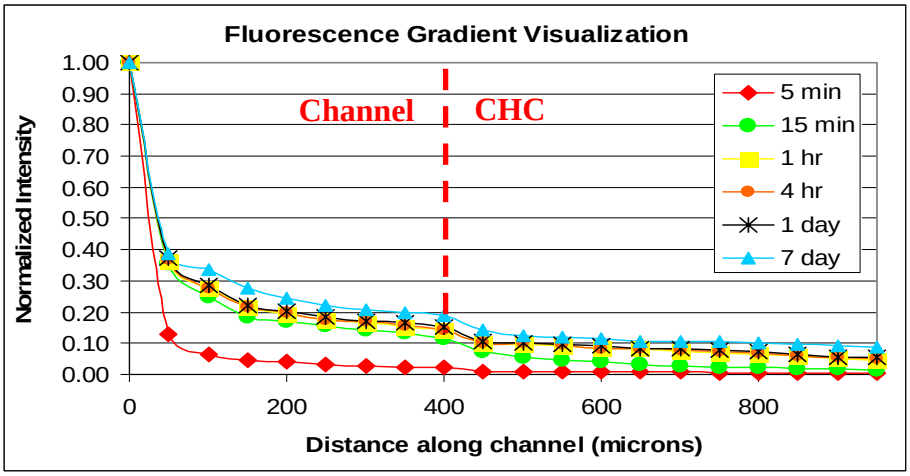

A

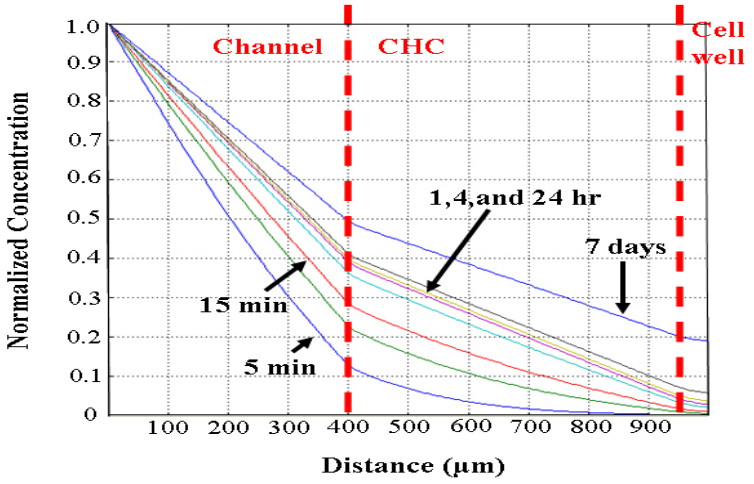

B

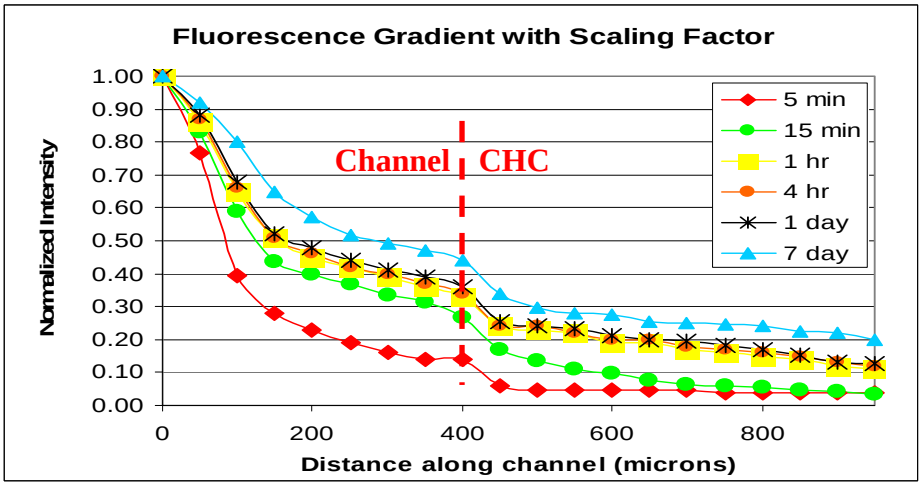

C

Figure 4-12. Gradient visualization using FITC-dextran; A) experimental gradient, B) theoretical gradient generated with Comsol Multiphysics 3.5a, C) experimental gradient with scaling factors. Note that the data for the 1 hr, 4 hr, and 1 day time points are close together for both plots (and appear to be on top of each other for plots A and C.

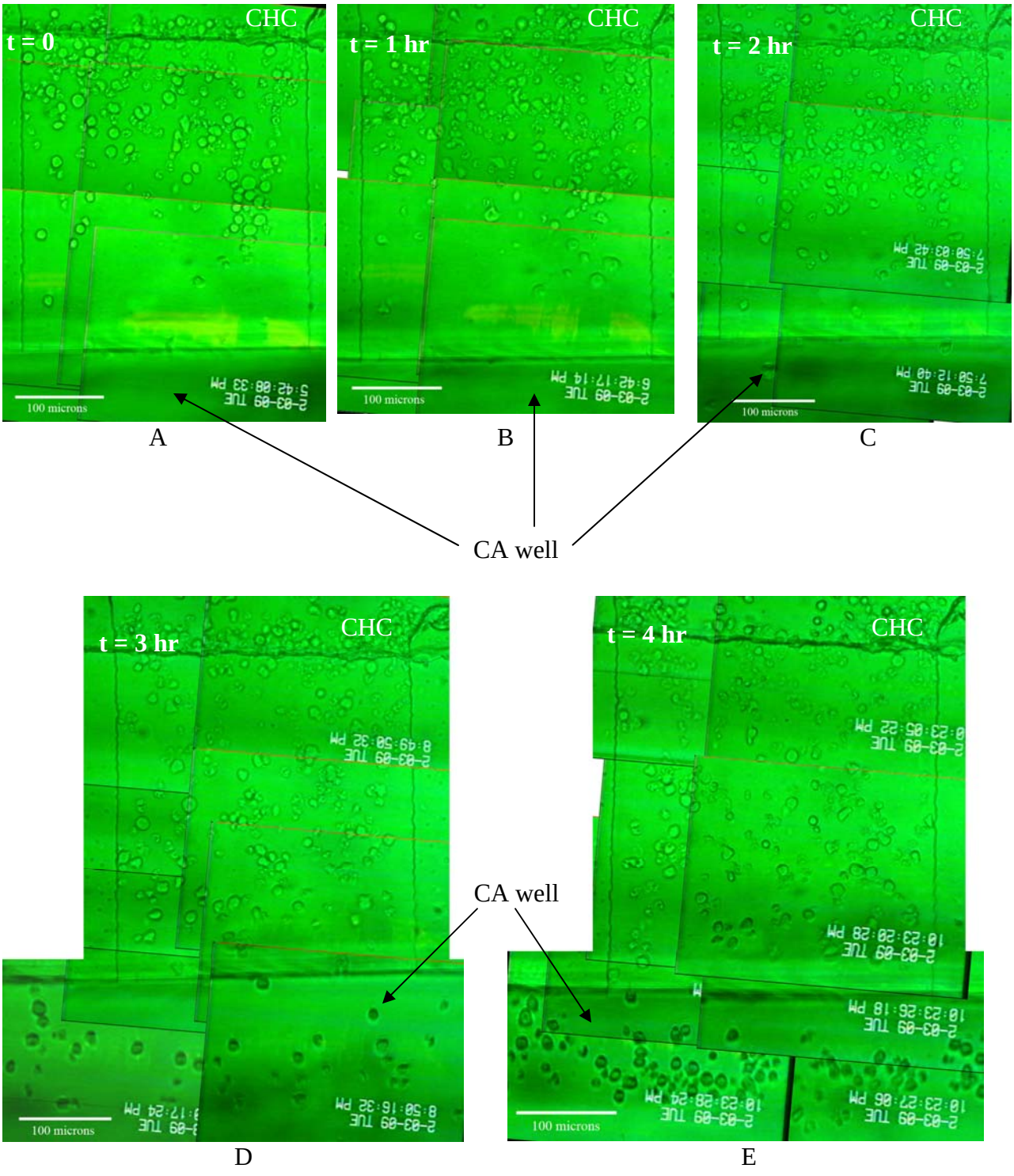

Figure 4-13. Jurkat cells migrating through the microchannel. 100 nM SDF-1 was loaded into the CA well at t = 0. A) t = 0, B) t = 1 hr, C) t = 2 hr, D) t = 3 hr, E) t = 4 hr. Scale bars are equal to 100 μm.

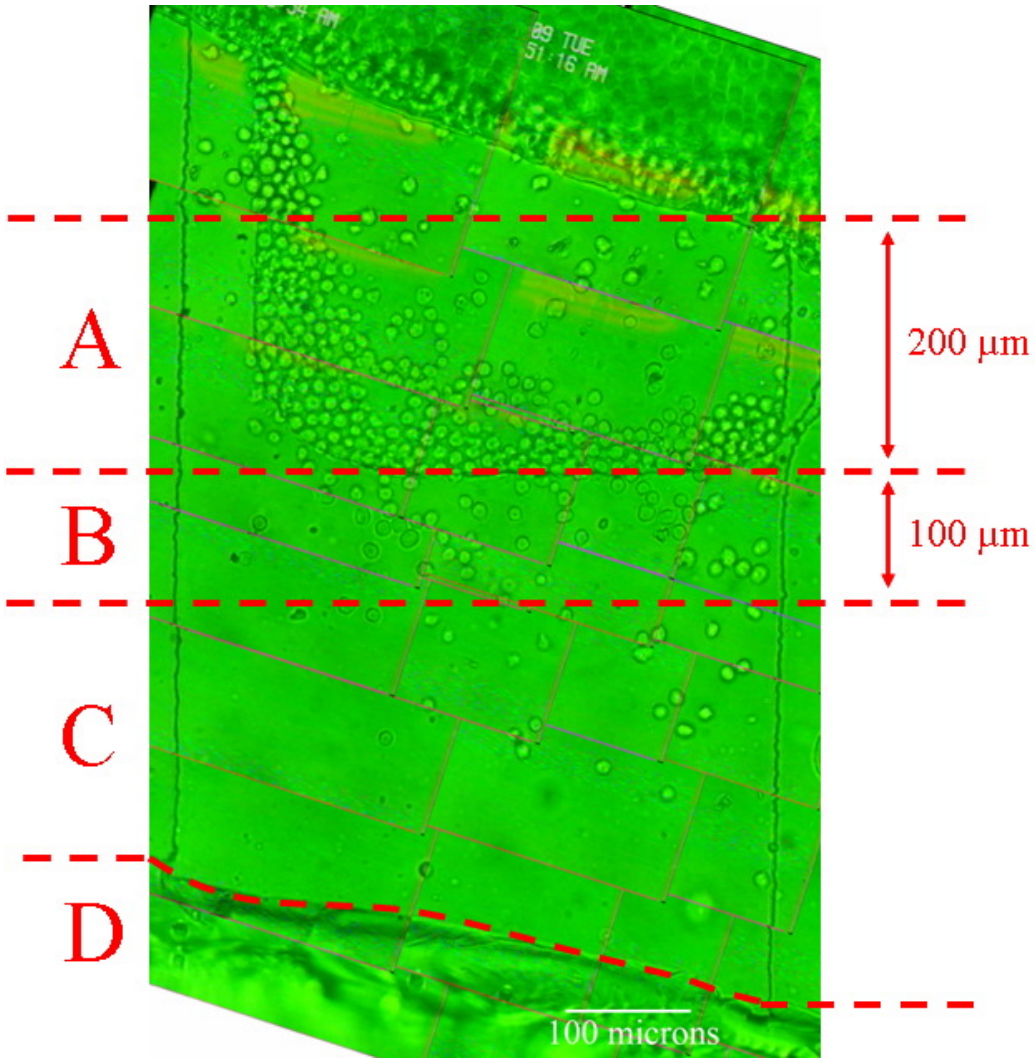

Figure 4-14. Micro-device divided into cell counting zones. Zone A represents the first 200 µm of the CHC, zone B is the first 100 µm of the channel, zone C is the remainder of the channel, and zone D is the CA well.

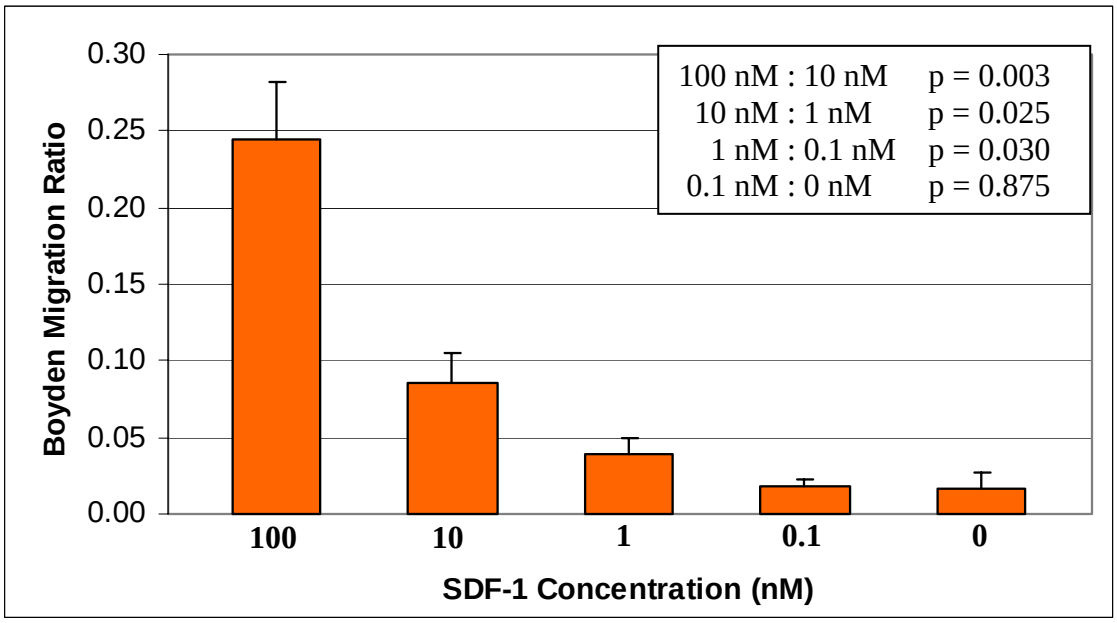

Figure 4-15. Results for Jurkat cell migration in Boyden chamber. n = 3 for all bars.

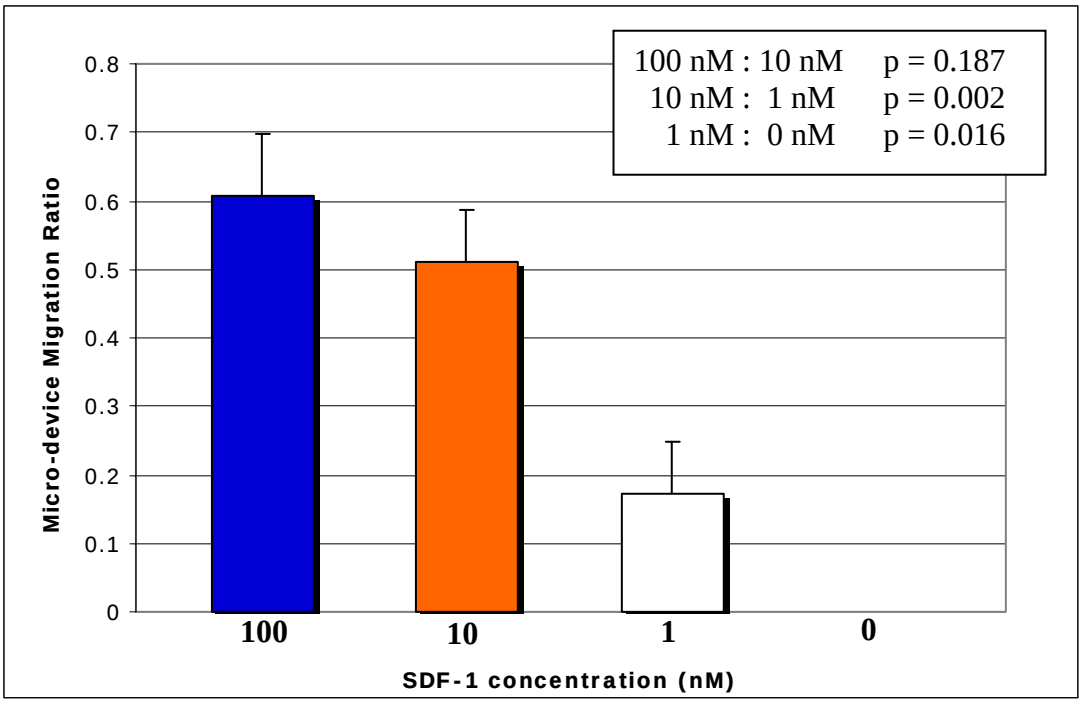

Figure 4-16. Effect of stromal cell-derived factor-1 (SDF-1) concentration on the migration ratio of Jurkat cells in the micro-devices. Tests performed in micro-devices with channel height = 10 μm. n values: 100 nM (3), 10 nM (4), 1 nM (3), 0 nM (3).

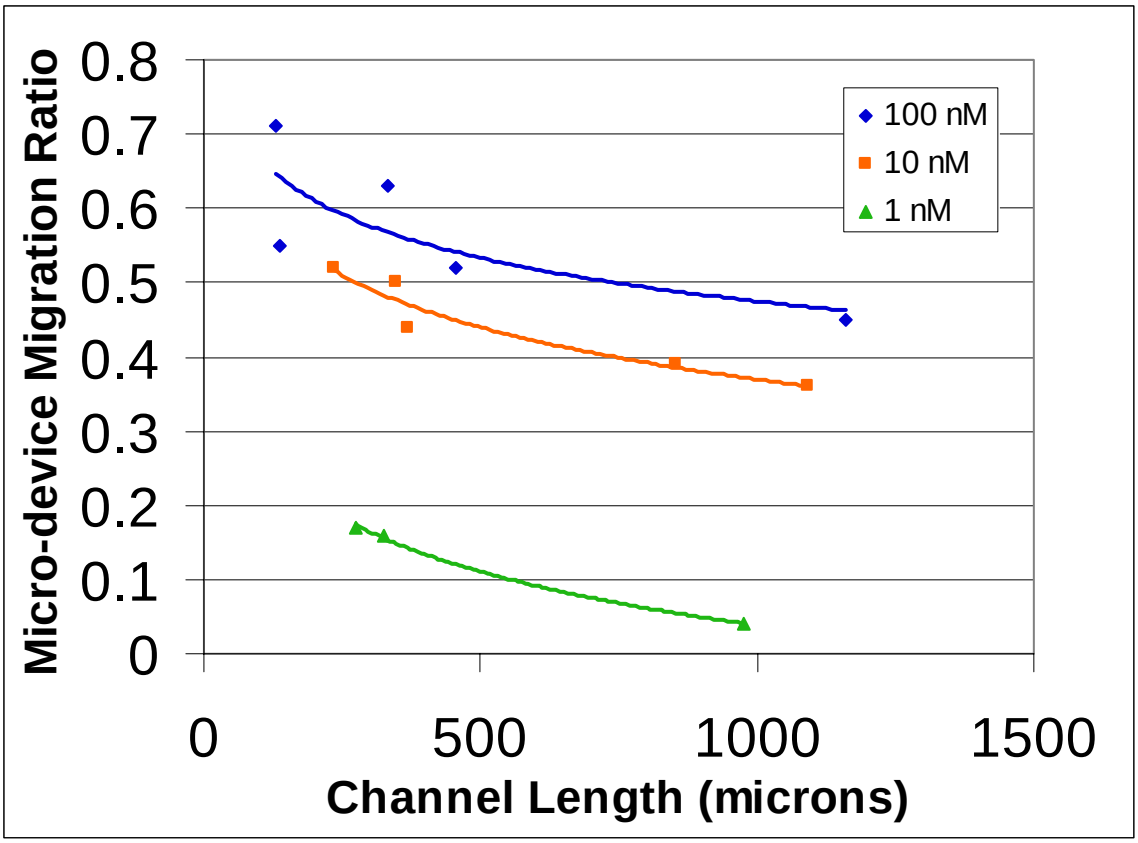

Figure 4-17. Effect of channel length on migration ratio in micro-devices. Tests were performed in channels with height = 14 μm, and SDF-1 concentrations of 1, 10, and 100 nM.

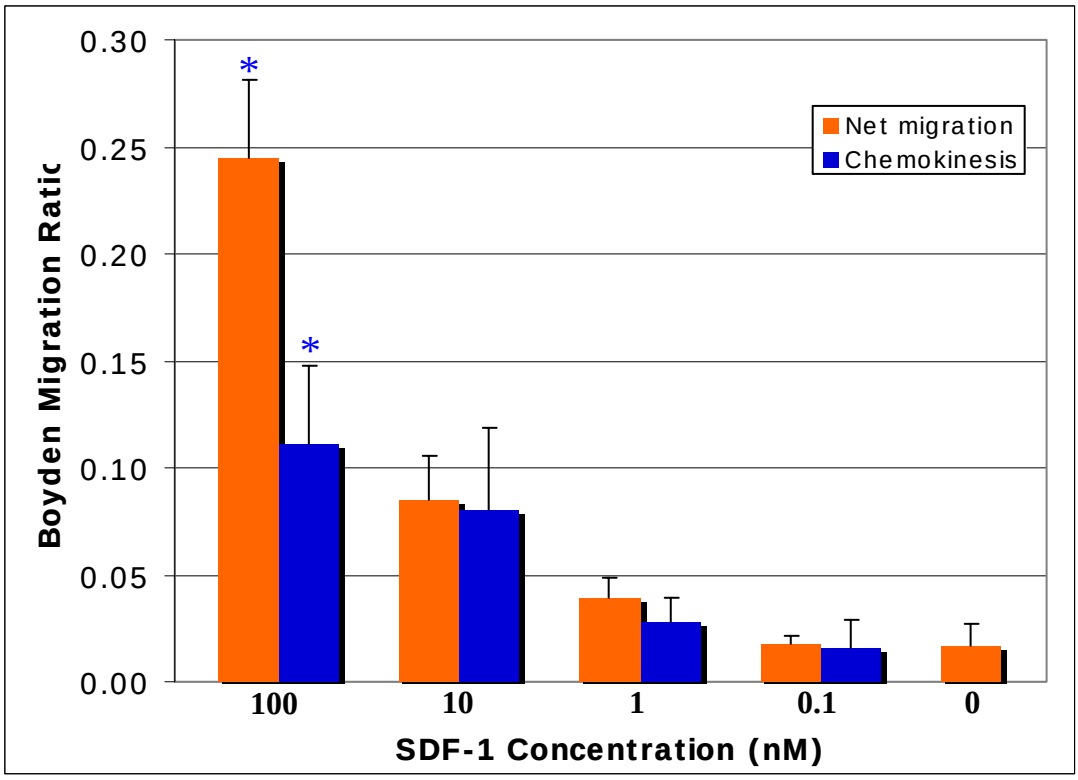

Figure 4-18. Boyden migration ratios for Jurkat cell "net migration" and "chemokinesis." n = 3 for all bars. * $p < 0.05$

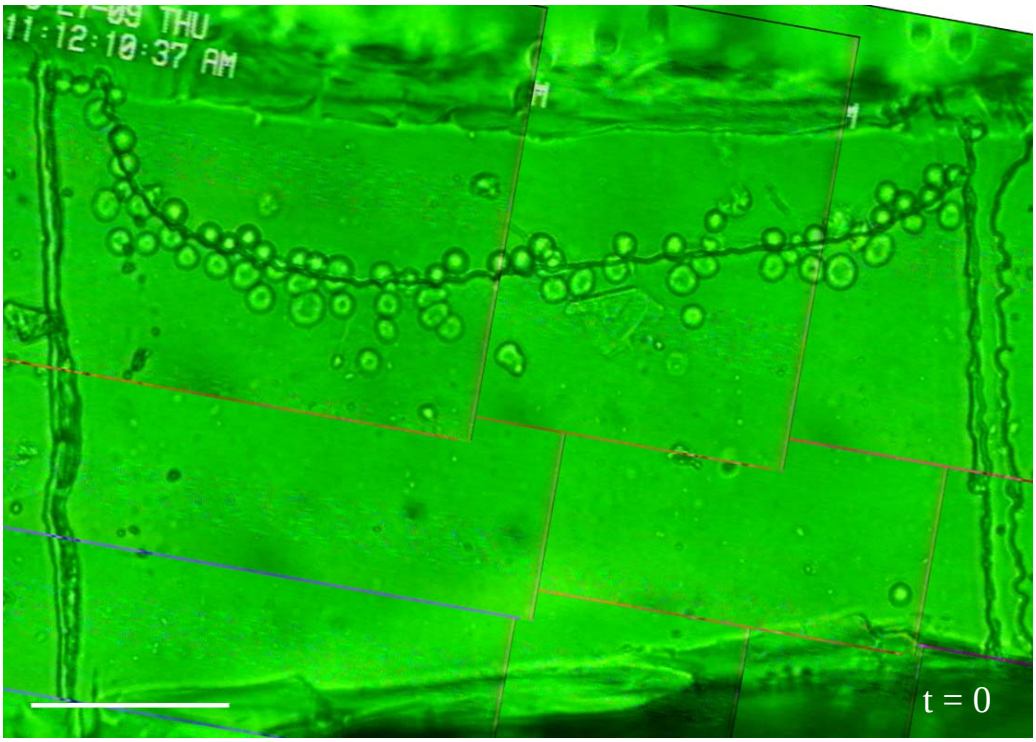

A

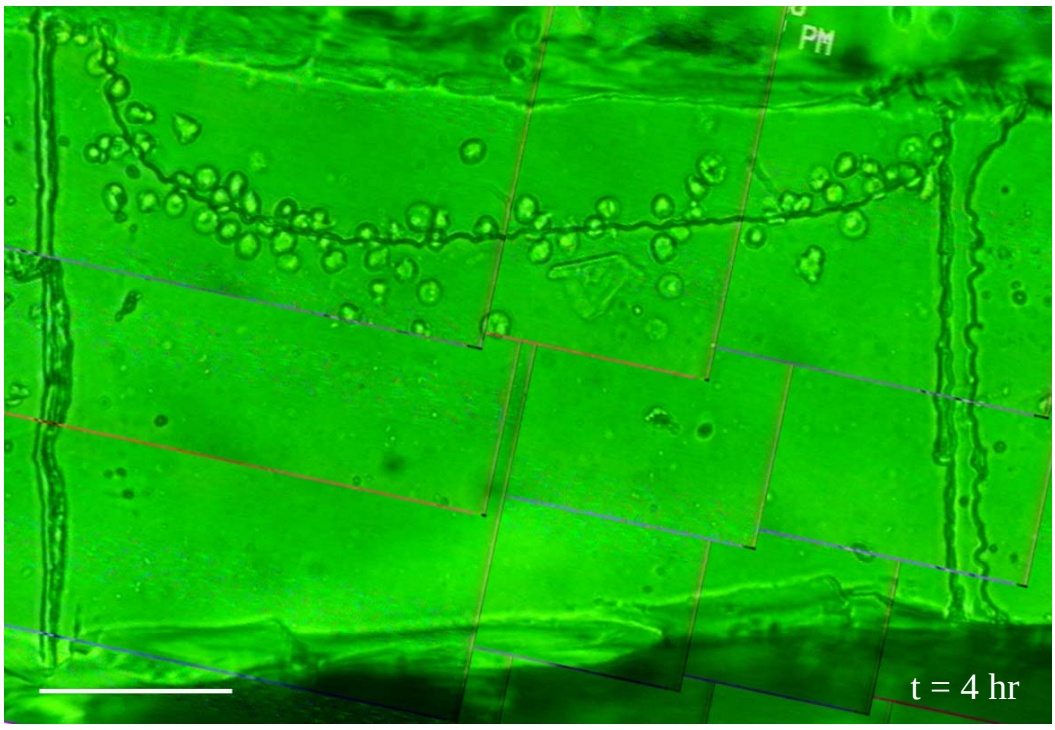

B

Figure 4-19. Chemokinesis (100 nM SDF-1) test performed in micro-device. Images taken at A) t = 0, and B) t = 4 hrs. Scale bar equals 100 μm.

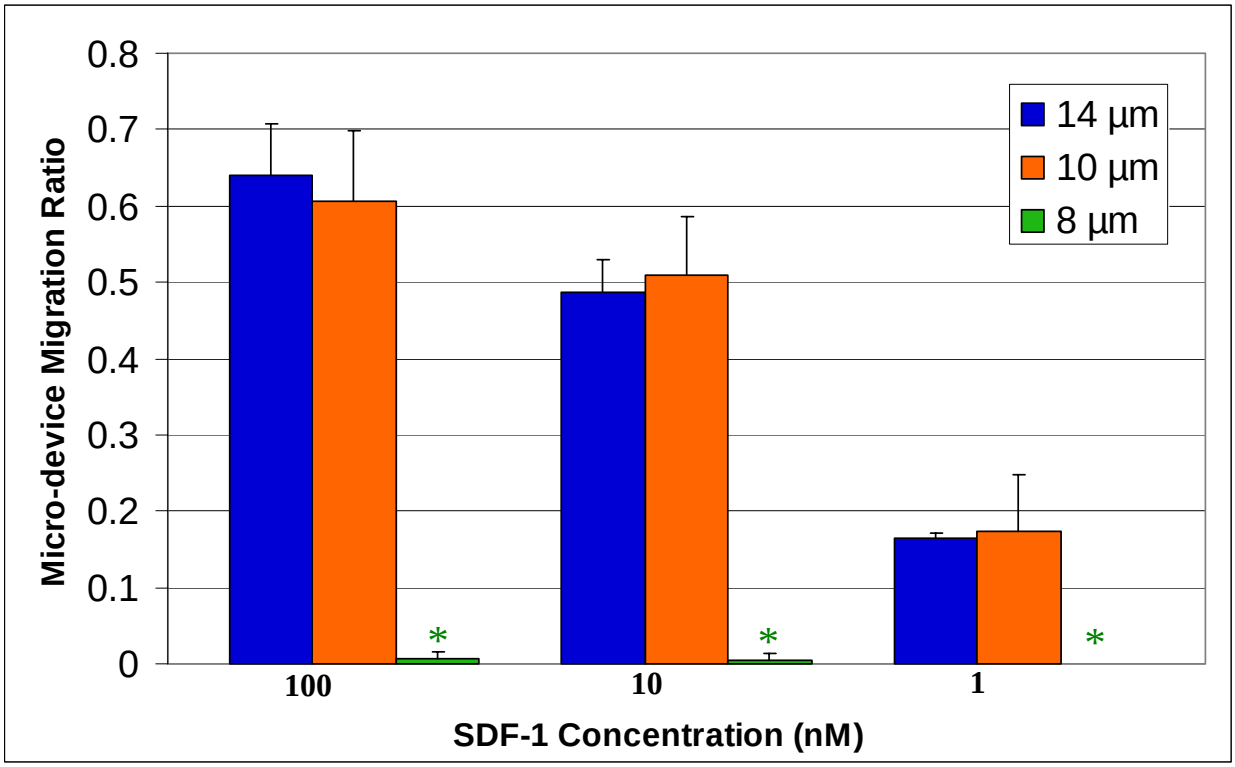

Figure 4-20. Jurkat cell migration ratios for 14, 10, and 8 µm channel heights. n values: 100 nM bars (4, 3, 6), 10 nM bars (3, 4, 6), 1 nM bars (2, 3, 6). * $p < 0.05$

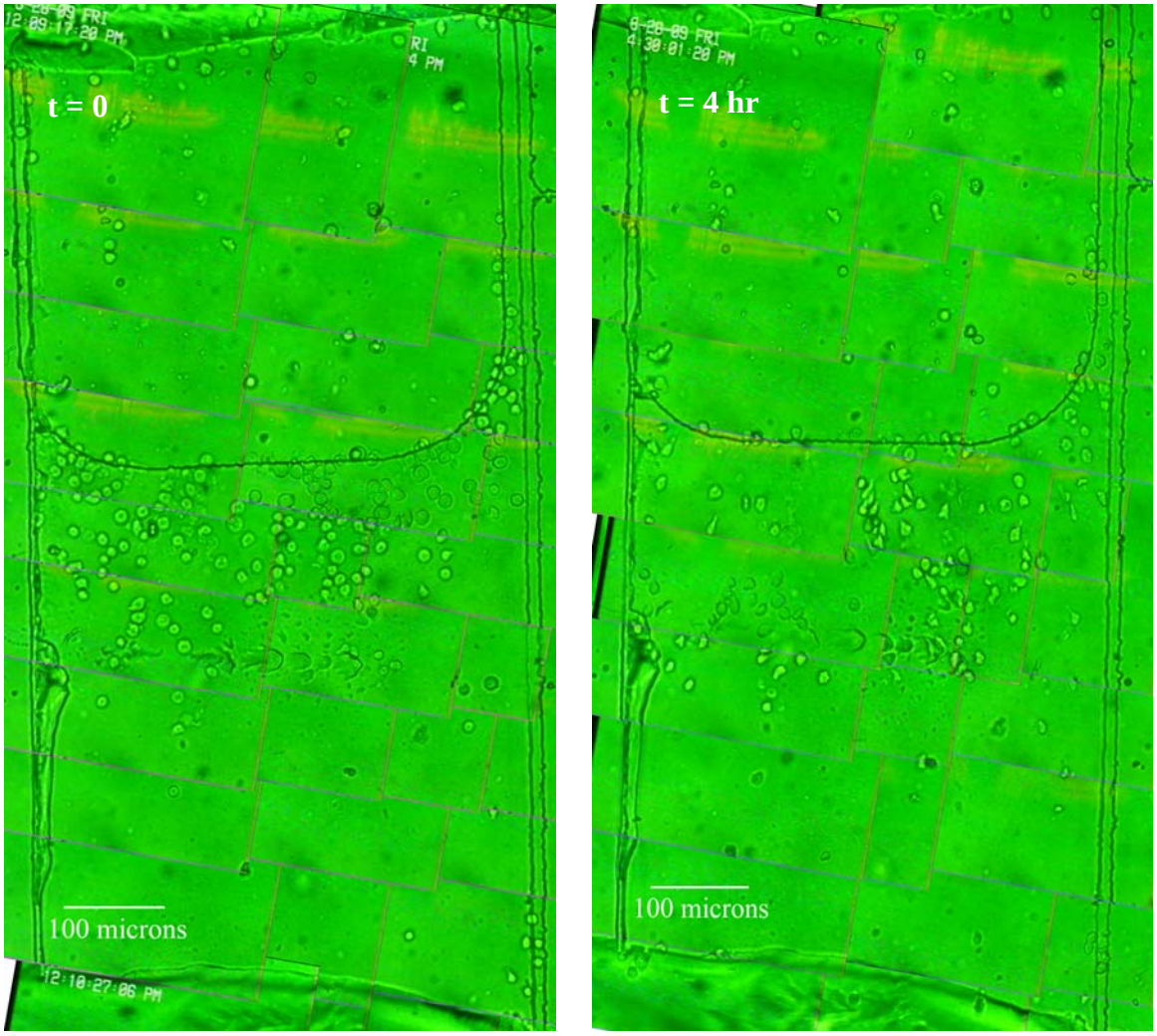

A B

Figure 4-21. Jurkat cell migration experiment performed in device with channel height = 8 μm and SDF-1 concentration equal to 10 nM. Images taken at A) t = 0 and B) t = 4 hr.

CHAPTER 5
CONCLUSION

We have developed a novel migration assay. The micro-scale dimensions of the device significantly reduce the volume of chemicals required by other migration assays, and by extension reduce the cost of each assay. Furthermore, the micro-scale dimensions of the channel force cells to deform in order to migrate. This mimics the physiologic environment and provides a more accurate measure of migratory function. In addition, the micro-device can be used to study migration in real-time, as well as quantify relative migration, which can be used to compare different cell populations. To date, no other assay has incorporated both of these modes of analysis. Specific conclusions concerning the development of the micro-scale migration assay are summarized below.

1. The micro-scale dimensions of the device reduce the volume of required chemoattractant by more than 10-fold (as compared to the Boyden chamber).

2. A gradient forms within 5 minutes of loading the device and is maintained for at least 7 days (as confirmed with fluorescence microscopy). This makes the device useful for long-term migration studies in which traditional methods (e.g. Boyden, Zigmond, agarose) cannot be used.

3. The height of the microchannel forces cells to deform before they can migrate through the device. 10 μm was found to be the ideal height for testing the migration of Jurkat cells.

4. The transparency of the PDMS allowed for direct viewing of cell deformation and migration through the device. Jurkat cells were observed to migrate approximately 66 μm/hr (in the presence of 100 nM SDF-1) through the microchannel.

5. Migration was quantified in terms of migration ratios. The migration ratio for Jurkat cells showed a direct relationship to SDF-1 concentration. These ratios are relative, as they can only be compared when all testing parameters are equal (e.g. micro-device dimensions, chemoattractant concentration, assay length, etc.).

6. The microchannel length, 100 μm, is too far for Jurkat cells to randomly migrate, therefore, the migration that was measured only included chemotaxis. Despite this, chemokinesis experiments can be performed in the micro-scale device by monitoring random migration within the channel via microscopy. The separation of chemotaxis and chemokinesis in the micro-device is an advantage over the Boyden chamber in which multiple experiments must be performed to isolate chemotaxis.

Jurkat cells were used in the development of this device. However, the device can be altered for use with other cell types. The channel height can be adjusted to accommodate any cell size. In addition, the length of the channel and CHC can be changed to produce gradients of varying steepness (see Appendix D). This expands the range of chemoattractant concentrations that can be used and the physiologic environments that can be modeled with this device.

CHAPTER 6
FUTURE WORK

Compare Micro-Scale Device Results to Boyden Chamber Results

Comparing the new micro-scale device to an accepted migration assay is needed to further test the design. The Boyden chamber is one of the most widely used migration assays. In this project, both devices were used to measure the migration ratio for Jurkat cells. However, the results obtained cannot be compared directly. The geometries of the two devices are very different. As a result, the number of cells that can migrate through each (within the same amount of time) varies. In addition, the gradients within each device are distinct. The gradient generated in the Boyden chamber is very steep at the start of the assay and decays rapidly over the course of a few hours. Consequently, cell migration rates are greater in the beginning and slow down as the assay progresses. Conversely, once the gradient forms in the micro-scale device it is relatively stable for several hours. As a result, cell migration rates remain fairly stable. These differences make it unacceptable to compare the migration ratios measured with the two assays.

In order to compare the micro-device to the Boyden chamber, an additional cell population (termed "population B") will need to be tested in each device. The migration ratio of the Jurkat cells (population A) should be compared to the migration ratio of population B, as measured in the micro-device. Similarly, the migration ratios for populations A and B should be measured with the Boyden chamber to determine which population migrates better. The ratios obtained from the different devices are relative measures of migration and cannot be compared to each other. However, the outcome (which cell population migrates better) should be the same for the Boyden chamber and the microfluidic migration device.

Reduce Variability in Micro-Device Geometry

The current device fabrication method allows for variation in channel and CHC lengths. This variation could be eliminated by using injection molding to fabricate the devices. Alternatively, the distance between the wells could be standardized by incorporating the wells into the photomask for rapid prototyping with PDMS. However, 2.5 mm tall wells cannot be etched into the thin silicon wafer. As an alternative, wells with a depth of 100 μm could be etched into the wafer to serve as a guide for hand-punching. A 2.5 mm layer of PDMS can be cured on top of the wafer. After peeling off the PDMS, the biopsy punch can be lined up with the well guides and punched through the PDMS layer to create the wells. This method will require an additional photomask and silicon master to be fabricated. However, it will still be economically feasible because it allows for rapid prototyping with PDMS.

The alternative fabrication method that has been suggested will not eliminate all variability; however it will reduce the variability substantially. More uniform channel and CHC lengths will mean that cell positioning times can be standardized and the "ideal" migration quantification method can be used. Furthermore, the standard deviation within the measured migration ratios should be reduced since the concentration gradients will be more consistent between devices.

Decrease Assay Time

Another improvement that could be made in the migration assay is a reduction in assay time. The assays that have been conducted so far were run for 4 hours so that they were comparable to Boyden chamber experiments. However, shortening this time would be advantageous. A migration rate of 66 ± 20 μm/hr was measured for the Jurkat cells. Therefore, 2 hours may be long enough for Jurkat cells to migrate through the 100 μm channel. It should be

noted that the length of the migration assay will change based on the cell type tested, as different cells migrate at different rates.

Improve Micro-Device Design and Protocol

Alter Micro-Device Dimensions

Shortening the microchannel length within the device will increase the number of cells that can migrate through in a given period of time. As a result, the assay time could be decreased. As previously mentioned, injection molding could be used to fabricate the micro-devices. This would allow for shorter channel lengths. Shortening the channel length to 50 μm would increase the number of cells that migrate into the CA well by more than 2 times (as compared to a channel length of 100 μm). This is due to the shorter distance the cells will traverse, as well as to increased migration rates due to a steeper concentration gradient (because the gradient gets steeper as the channel length is decreased). The "altered" channel length was chosen to be 50 μm (and not any shorter) to ensure that chemokinesis is not measured in the migration assay.

If the channel length is decreased, the CHC length should also be decreased. For a 50 μm channel, a 100 μm CHC should be chosen. This will maintain a steep gradient within the channel while still providing enough space to collect cells.

Decreasing the volume of the CA and cell wells will decrease assay cost by reducing the volume of chemicals required to run each assay. The diameter of each well could be decreased to 2 mm, which would decrease the volume by more than 3 times. Chemoattractant and cell loading into wells this small could be done with a syringe instead of a pipetter.

Incorporate Multiple Channels into Design

Incorporating multiple channels into each device would increase throughput. In addition, it would provide multiple channels for real-time analysis without increasing the volume of chemicals or cells required. The current design is limited to one channel because a circular

punch is used to create the wells. The curved edge of the well makes it impossible to have multiple channels and CHCs with a uniform length. This could be remedied by using a square punch. This would create a straight edge and result in uniform lengths for the channels and CHCs. Based on a well width of 2 mm, 3 channels (each 500 μm wide) could be incorporated into each device.

Alter Well Geometry to Facilitate Cell Positioning

Tilting the micro-devices to position cells within the CHC is tedious and adds 30 min to each assay. The well geometry could be altered to facilitate cell positioning and eliminate the tilting step. In the current design, the walls of the cell well are perpendicular to the roof of the CHC and channel. If the walls are changed to slopes they will act as a funnel to position the cells within the CHC (see Figure 6-1). This will combine the cell loading and positioning steps and only take a matter of seconds.

Automate Cell Counting

The current cell staining and counting method is easy and does not require special equipment. However, it can take a long time to count individual cells. This process can be automated by labeling the cells with a fluorescent dye prior to being loaded into the micro-devices, and then using a fluorescence plate reader to measure the fluorescence intensity in the CA well at the end of the assay. The measured intensity is a relative measure of the number of cells in the well, and can be used to compare the results from multiple assays.

Automate Real-Time Analysis of Migration

In addition to automating cell counting at the end of the assay, fluorescence labeling of the cells could be used to automate real-time migration analysis throughout the assay. Cell tracking software (such as Imaris Track by Bitplane Inc. (MN, USA)) can be used to track individual cell paths. This will require a microscope equipped with fluorescence capabilities, as well as an

image acquisition software such as Pinnacle (Pinnacle Systmes, CA, USA). In addition, a lower power objective should be used so that the entire channel can be viewed at one time. Due to availability, a 20x objective was used for this project. As a result, the channel had to be scanned to produce multiple images, which were then aligned to produce an image of the complete channel. A 10x objective with an adjustable focal length would allow the entire channel to be viewed at once, thereby allowing for real-time cell tracking throughout the channel.

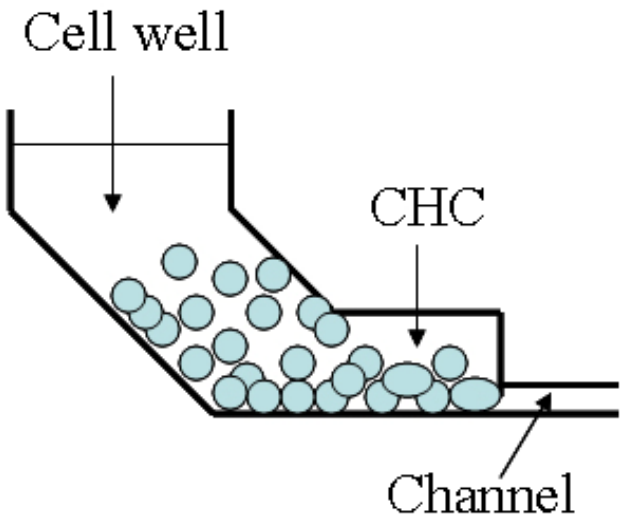

Figure 6-1. Schematic of altered cell well geometry. The sloped walls of the cell well act as a funnel to position the cells within the CHC. Schematic not drawn to scale.

APPENDIX A
JURKAT CELL MEASUREMENTS

Table A-1. Measured diameters for Jurkat cells, un-deformed and deformed in a 10 μm tall channel

Un-deformed Jurkat cells		Deformed Jurkat cells (in 10 μm channel)	
Cell #	Diameter (μm)	Cell #	Diameter (μm)
1	15.4	1	15
2	13	2	17.3
3	12.7	3	18.7
4	12.7	4	16.8
5	11.7	5	16.8
6	17.1	6	14.5
7	12.7	7	17.3
8	17.1	8	16.4
9	13.4	9	14
10	14.1	10	16.4
11	13	11	17.3
12	12.3	12	13.6
13	11.3	13	14.5
14	13	14	14
15	13.4	15	16.4
16	12.3	16	15.9
17	10.3	17	16.8
18	12.7	18	14.5
19	13.7	19	15.4
20	14.4	20	13.1
21	12.3	21	15
22	12	22	16.4
23	13	23	16.4
24	11.3	24	15
25	16.8	25	14
26	11.7	26	18.7
27	11.7	27	13.6
28	15.1	28	17.3
29	13.4	29	13.6
30	12.3	30	15.4
Average diameter: 13.2 ± 1.7 μm		Average diameter: 15.7 ± 1.5 μm	

APPENDIX B
COMSOL MULTIPHYSICS SIMULATIONS

Diffusion simulations were performed using Comsol Multiphysics v.3.5. The schematic and conditions that were used are given in Figure B-1. The CA well was not included in the schematic because it acts as an infinite source, therefore, the concentration at the junction of the channel and CA well (boundary 1 in Figure B-1) remains constant. The concentrations that were calculated were normalized, so the concentration at boundary 1 was set as c=1. A representative diffusion analysis and the corresponding cross-sectional plot are given in Figure B-2 and Figure B-3.

Model:
2-D, time-dependent, diffusion

Equation:

$$\frac{\partial c}{\partial t} = D\nabla^2 c$$

Boundary settings:

1	c=1
2	Insulation
3	Insulation
4	Insulation
5	Insulation
6	Insulation
7	Insulation

Subdomain settings:
isotropic diffusion
Diffusion constant:
$D_{FITC\text{-}dextran} = 1.7 \times 10^{-6}\ cm^2/s$

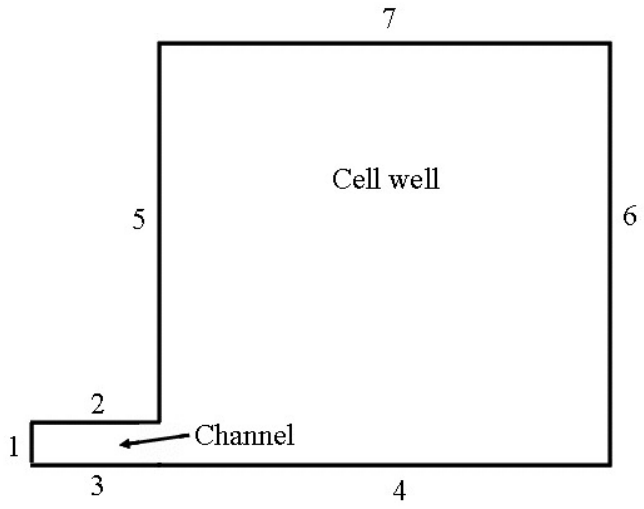

Figure B-1. Schematic and parameter inputs used for Comsol Multiphysics (v.3.5) diffusion simulations.

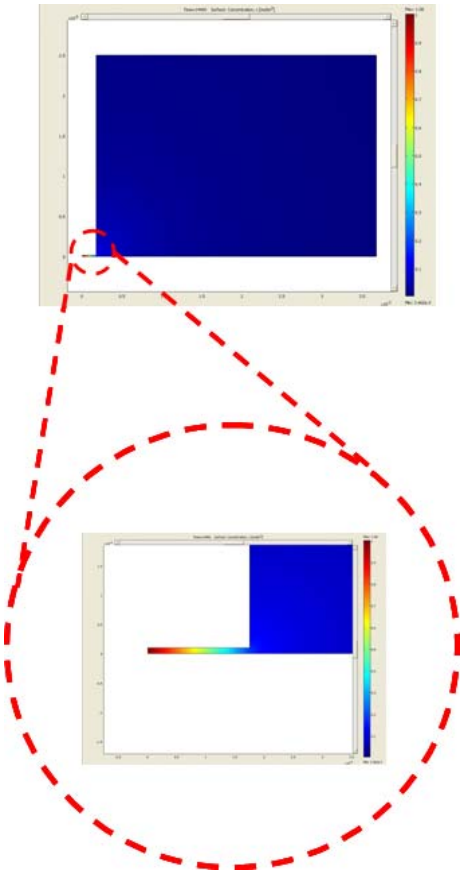

Figure B-2. Representative Comsol Multiphysics output. The different colors within the channel represent varying concentration along the channel length.

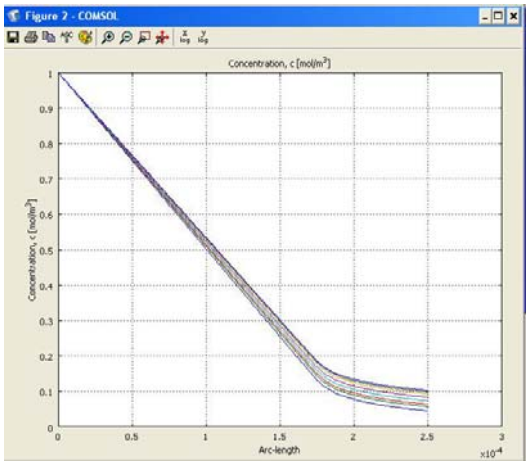

Figure B-3. Plot of concentration versus distance from the CA well, for multiple times points.

APPENDIX C
CALCULATIONS

- Calculation for force exerted on the fluid within the channel and CHC:

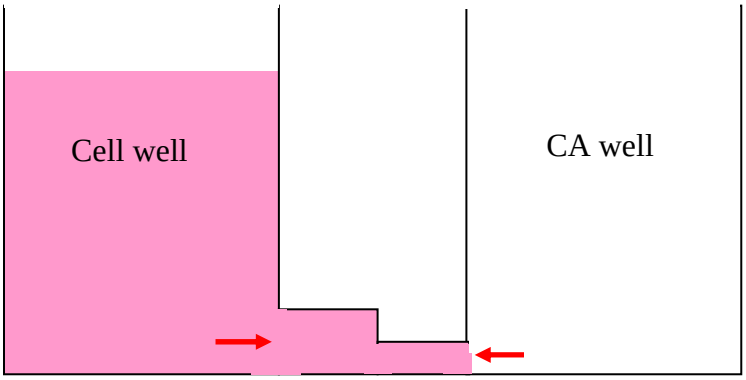

Figure C-1. Schematic illustrating force calculations within the micro-device. Red arrows indicate where force was calculated.

- Force exerted on cell well end of CHC:
  - Calculate pressure exerted by media in cell well:

$$P = \rho g h$$

    - ρ for water at 30°C (1000 kg/m^3) was used as an approximation for ρ of SFM
    - Calculate h (based on volume of fluid added to cell well, 20 μL):

$$V_{cylinder} = \pi r^2 h$$

$$h = \frac{(20\mu L)\left(\frac{1L}{10^6 \mu L}\right)\left(\frac{1m^3}{1000L}\right)}{\pi\left(1.75x10^{-3}m\right)^2} = 2x10^{-3}m$$

$$P = \left(1000\frac{kg}{m^3}\right)\left(9.8\frac{m}{s^2}\right)\left(2x10^{-3}m\right) = 19.6\frac{kg}{m \bullet s^2}$$

- Calculate force:

$$F = (P)(A)$$

- Calculate A (area) for CHC entrance (24 μm x 500 μm) :

$$A = (2.4x10^{-5}m)(5x10^{-4}m) = 1.2x10^{-8}m^2$$

$$F = \left(19.6\frac{kg}{m \bullet s^2}\right)(1.2x10^{-8}m^2) = \boxed{2.35x10^{-7}N}$$

- Force exerted on CA well end of channel:

$$F = (P)(A)$$

- Calculate A (area) for channel entrance (10 μm x 500 μm) :

$$A = (1x10^{-5}m)(5x10^{-4}m) = 5x10^{-9}m^2$$

$$F = \left(101325\frac{kg}{m \bullet s^2}\right)(5x10^{-9}m^2) = \boxed{5.07x10^{-4}N}$$

- Sample calculations to show effect of fluid height difference in cell and CA wells:
  - Calculate pressure drop:

$$\Delta P = \rho g \Delta h$$

  - Calculate Δh based on a volume difference of 1 μL between the 2 wells (20 μL and 19 μL:

$$V_{cylinder} = \pi r^2 h$$

    - 20 μL:

$$h = \frac{(20\mu L)\left(\frac{1L}{10^6 \mu L}\right)\left(\frac{1m^3}{1000L}\right)}{\pi\left(1.75x10^{-3}m\right)^2} = 2x10^{-3}m$$

- 19 μL:

$$h = \frac{(19\mu L)\left(\frac{1L}{10^6 \mu L}\right)\left(\frac{1m^3}{1000L}\right)}{\pi\left(1.75x10^{-3}m\right)^2} = 1.97x10^{-3}m$$

$$\Delta h = \left(2x10^{-3}m\right) - \left(1.97x10^{-3}m\right) = 3x10^{-5}m$$

$$\Delta P = \left(1000\frac{kg}{m^3}\right)\left(9.8\frac{m}{s^2}\right)\left(3x10^{-5}m\right) = 2.94x10^{-1}\frac{kg}{m \bullet s^2}$$

- Calculate resistance (L = 100 μm, w = 500 μm, h = 10 μm):

$$R = \frac{12\mu L}{wh^3}$$

- μ for water at 30°C ($7.978x10^{-4}$ kg/m*s) was used as an approximation for μ of SFM

$$R = \frac{12\left(7.978x10^{-4}\frac{kg}{m \bullet s}\right)\left(1x10^{-4}m\right)}{\left(5x10^{-4}m\right)\left(1x10^{-5}m\right)^3} = 1.915x10^{12}\frac{kg}{m^4 \bullet s}$$

- Calculate volumetric flow rate, Q:

$$Q = \frac{\Delta P}{R}$$

$$Q = \frac{\left(2.94x10^{-1}\frac{kg}{m \bullet s^2}\right)}{\left(1.915x10^{12}\frac{kg}{m^4 \bullet s}\right)} = 1.535x10^{-13}\frac{m^3}{s} = 1.535x10^{5}\frac{\mu m^3}{s}$$

APPENDIX D
MICRO-DEVICE DIFFUSION ANALYSIS

Comsol Multiphysics 3.5a was used to simulate diffusion within micro-scale migration devices with varying dimensions. Combinations of the following dimensions (all in μm) were used: channel length (10, 20, 50, 100, 200, 300, 400, 500, 600, 750, 1000), channel height (6, 8, 10, 12), CHC length (100, 200), and CHC height (20). The normalized concentrations at the channel and CHC inlet, as well as the slope ((reported value) x 10^{-3}) of the gradient in the channel and CHC are given in Table D-1. This table can be used to quickly examine the effects of altering the various dimensions of the device.

Table D-1. Diffusion simulation results for micro-scale device with varied dimensions. All reported dimensions (length and height) have units of μm. The normalized concentration values are unitless. The slopes are (value reported in table) x 10^{-3}.

Channel		CHC			Channel		CHC	
Length	Height	Length	Height		Inlet conc.	Slope	Inlet conc.	Slope
10	6	100	20		0.83	17	0.31	5.2
10	6	200	20		0.88	12	0.2	3.4
10	8	100	20		0.87	13	0.32	5.5
10	8	200	20		0.9	10	0.21	3.5
10	10	100	20		0.88	12	0.34	5.4
10	10	200	20		0.91	9	0.21	3.5
10	12	100	20		0.9	10	0.34	5.6
10	12	200	20		0.92	8	0.22	3.5
20	6	100	20		0.72	14	0.27	4.5
20	6	200	20		0.81	9.5	0.19	3.1
20	8	100	20		0.77	11.5	0.29	4.8
20	8	200	20		0.82	9	0.2	3.1
20	10	100	20		0.81	9.5	0.3	5.1
20	10	200	20		0.86	7	0.2	3.3
20	12	100	20		0.84	8	0.32	5.2
20	12	200	20		0.88	6	0.22	3.3

Table D-1. Continued

Channel		CHC			Channel		CHC	
Length	Height	Length	Height		Inlet conc.	Slope	Inlet conc.	Slope
50	6	100	20		0.51	9.8	0.28	2.3
50	6	200	20		0.62	7.6	0.14	2.4
50	8	100	20		0.58	8.4	0.22	3.6
50	8	200	20		0.69	6.2	0.15	2.7
50	10	100	20		0.63	7.4	0.28	3.5
50	10	200	20		0.73	5.4	0.17	2.8
50	12	100	20		0.66	6.8	0.2	4.6
50	12	200	20		0.76	4.8	0.28	2.4
100	6	100	20		0.34	6.6	0.13	2.1
100	6	200	20		0.44	5.6	0.1	1.7
100	8	100	20		0.4	6	0.15	2.5
100	8	200	20		0.52	4.8	0.13	2
100	10	100	20		0.46	5.4	0.18	2.8
100	10	200	20		0.57	4.3	0.13	2.2
100	12	100	20		0.5	5	0.19	3.1
100	12	200	20		0.61	3.9	0.15	2.3
200	6	100	20		0.2	4	0.08	1.2
200	6	200	20		0.29	3.6	0.07	1.1
200	8	100	20		0.24	3.8	0.09	1.5
200	8	200	20		0.34	3.3	0.08	1.3
200	10	100	20		0.28	3.6	0.12	1.6
200	10	200	20		0.4	3	0.09	1.6
200	12	100	20		0.33	3.4	0.13	2
200	12	200	20		0.44	2.8	0.1	1.7
300	6	100	20		0.13	2.9	0.06	0.7
300	6	200	20		0.22	2.6	0.05	0.9
300	8	100	20		0.18	2.7	0.07	1.1
300	8	200	20		0.26	2.5	0.05	1.1
300	10	100	20		0.22	2.6	0.08	1.4
300	10	200	20		0.31	2.3	0.08	1.2
300	12	100	20		0.24	2.5	0.09	1.5
300	12	200	20		0.34	2.2	0.08	1.3
400	6	100	20		0.11	2.2	0.04	0.7
400	6	200	20		0.17	2.1	0.04	0.7
400	8	100	20		0.14	2.2	0.04	1
400	8	200	20		0.21	2	0.05	0.8
400	10	100	20		0.17	2.1	0.07	1
400	10	200	20		0.25	1.9	0.06	1
400	12	100	20		0.2	2	0.08	1.2
400	12	200	20		0.29	1.8	0.07	1.1

Table D-1. Continued

Channel		CHC			Channel		CHC	
Length	Height	Length	Height		Inlet conc.	Slope	Inlet conc.	Slope
400	6	100	20		0.11	2.2	0.04	0.7
400	6	200	20		0.17	2.1	0.04	0.7
400	8	100	20		0.14	2.2	0.04	1
400	8	200	20		0.21	2	0.05	0.8
400	10	100	20		0.17	2.1	0.07	1
400	10	200	20		0.25	1.9	0.06	1
400	12	100	20		0.2	2	0.08	1.2
400	12	200	20		0.29	1.8	0.07	1.1
500	6	100	20		0.09	1.8	0.03	0.6
500	6	200	20		0.14	1.7	0.02	0.6
500	8	100	20		0.11	1.8	0.04	0.7
500	8	200	20		0.17	1.7	0.03	0.7
500	10	100	20		0.14	1.7	0.04	1
500	10	200	20		0.21	1.6	0.04	0.9
500	12	100	20		0.16	1.7	0.06	1
500	12	200	20		0.24	1.5	0.06	0.9
750	6	100	20		0.06	1.3	0.02	0.4
750	6	200	20		0.09	1.2	0.02	0.4
750	8	100	20		0.07	1.2	0.02	0.5
750	8	200	20		0.12	1.2	0.02	0.5
750	10	100	20		0.1	1.2	0.03	0.7
750	10	200	20		0.14	1.2	0.03	0.6
750	12	100	20		0.12	1.2	0.05	0.7
750	12	200	20		0.17	1.1	0.03	0.7
1000	6	100	20		0.05	1	0.01	0.4
1000	6	200	20		0.07	0.9	0.01	0.3
1000	8	100	20		0.06	0.9	0.02	0.4
1000	8	200	20		0.09	0.9	0.02	0.4
1000	10	100	20		0.08	0.9	0.02	0.6
1000	10	200	20		0.11	0.9	0.02	0.5
1000	12	100	20		0.09	0.9	0.03	0.6
1000	12	200	20		0.13	0.9	0.02	0.6

LIST OF REFERENCES

1. Guan, J. L. in *Cell Migration: Developmental Methods and Protocols* 3-6 (Humana Press Inc., Totowa, New Jersey, 2005).

2. Leber, T. Uber die Entstehung der Entzundung und die Wirkung der entzundungerregenden Schadlichkeiten. *Fortschr. Med.* **4**, 460 (1888).

3. Ketchel, M. M. & Favour, C. B. The acceleration and inhibition of migration of human leucocytes in vitro by plasma protein fractions. *J. Exp. Med.* **101**, 647-663 (1955).

4. Zigmond, S. H. & Hirsch, J. G. Leukocyte locomotion and chemotaxis. New methods for evaluation, and demonstration of a cell-derived chemotactic factor. *J. Exp. Med.* **137**, 387-410 (1973).

5. Hadjout, N., Laevsky, G., Knecht, D. A. & Lynes, M. A. Automated real-time measurement of chemotactic cell motility. *BioTechniques* **31**, 1130-1138 (2001).

6. Zicha, D., Dunn, G. A. & Brown, A. F. A new direct-viewing chemotaxis chamber. *J. Cell. Sci.* **99 (Pt 4)**, 769-775 (1991).

7. Dunn, G. A. Using the Dunn chemotaxis chamber (Hawksley DCC100). www.hawksley.co.uk. Accessed October 2007.

8. Nelson, R. D., Quie, P. G. & Simmons, R. L. Chemotaxis under agarose: a new and simple method for measuring chemotaxis and spontaneous migration of human polymorphonuclear leukocytes and monocytes. *J. Immunol.* **115**, 1650-1656 (1975).

9. Newton-Nash, D. K., Tonellato, P., Swiersz, M. & Abramoff, P. Assessment of chemokinetic behavior of inflammatory lung macrophages in a linear under-agarose assay. *J. Leukoc. Biol.* **48**, 297-305 (1990).

10. Boyden, S. The chemotactic effect of mixtures of antibody and antigen on polymorphonuclear leucocytes. *J. Exp. Med.* **115**, 453-466 (1962).

11. NeuroProbe. ChemoTx® disposable chemotaxis system. www.neuroprobe.com. Accessed October 2007.

12. Skierczynski, B. A., Usami, S., Chien, S. & Skalak, R. Active motion of polymorphonuclear leukocytes in response to chemoattractant in a micropipette. *J. Biomech. Eng.* **115**, 503-509 (1993).

13. Usami, S., Wung, S. L., Skierczynski, B. A., Skalak, R. & Chien, S. Locomotion forces generated by a polymorphonuclear leukocyte. *Biophys. J.* **63**, 1663-1666 (1992).

14. Abhyankar, V. V., Lokuta, M. A., Huttenlocher, A. & Beebe, D. J. Characterization of a membrane-based gradient generator for use in cell-signaling studies. *Lab. Chip* **6**, 389-393 (2006).

15. Saadi, W. *et al*. Generation of stable concentration gradients in 2D and 3D environments using a microfluidic ladder chamber. *Biomed. Microdevices* **9**, 627-635 (2007).

16. Frevert, C. W., Boggy, G., Keenan, T. M. & Folch, A. Measurement of cell migration in response to an evolving radial chemokine gradient triggered by a microvalve. *Lab. Chip* **6**, 849-856 (2006).

17. Irimia, D. *et al*. Microfluidic system for measuring neutrophil migratory responses to fast switches of chemical gradients. *Lab. Chip* **6**, 191-198 (2006).

18. Li Jeon, N. *et al*. Neutrophil chemotaxis in linear and complex gradients of interleukin-8 formed in a microfabricated device. *Nat. Biotechnol.* **20**, 826-830 (2002).

19. Lin, F. *et al*. Neutrophil migration in opposing chemoattractant gradients using microfluidic chemotaxis devices. *Ann. Biomed. Eng.* **33**, 475-482 (2005).

20. Tharp, W. G. *et al*. Neutrophil chemorepulsion in defined interleukin-8 gradients in vitro and in vivo. *J. Leukoc. Biol.* **79**, 539-554 (2006).

21. Saadi, W., Wang, S. J., Lin, F. & Jeon, N. L. A parallel-gradient microfluidic chamber for quantitative analysis of breast cancer cell chemotaxis. *Biomed. Microdevices* **8**, 109-118 (2006).

22. Wang, S. J., Saadi, W., Lin, F., Minh-Canh Nguyen, C. & Li Jeon, N. Differential effects of EGF gradient profiles on MDA-MB-231 breast cancer cell chemotaxis. *Exp. Cell Res.* **300**, 180-189 (2004).

23. Shamloo, A., Ma, N., Poo, M. M., Sohn, L. L. & Heilshorn, S. C. Endothelial cell polarization and chemotaxis in a microfluidic device. *Lab. Chip* **8**, 1292-1299 (2008).

24. Cheng, S. Y. *et al*. A hydrogel-based microfluidic device for the studies of directed cell migration. *Lab. Chip* **7**, 763-769 (2007).

25. Walker, G. M. *et al*. Effects of flow and diffusion on chemotaxis studies in a microfabricated gradient generator. *Lab. Chip* **5**, 611-618 (2005).

26. Chaw, K. C., Manimaran, M., Tay, F. E. & Swaminathan, S. Matrigel coated polydimethylsiloxane based microfluidic devices for studying metastatic and non-metastatic cancer cell invasion and migration. *Biomed. Microdevices* **9**, 597-602 (2007).

27. Chaw, K. C., Manimaran, M., Tay, F. E. & Swaminathan, S. A quantitative observation and imaging of single tumor cell migration and deformation using a multi-gap microfluidic device representing the blood vessel. *Microvasc. Res.* **72**, 153-160 (2006).

28. Kanegasaki, S. *et al*. A novel optical assay system for the quantitative measurement of chemotaxis. *J. Immunol. Methods* **282**, 1-11 (2003).

29. Nitta, N., Tsuchiya, T., Yamauchi, A., Tamatani, T. & Kanegasaki, S. Quantitative analysis of eosinophil chemotaxis tracked using a novel optical device -- TAXIScan. *J. Immunol. Methods* **320**, 155-163 (2007).

30. Radmacher, M., Fritz, M., Kacher, C. M., Cleveland, J. P. & Hansma, P. K. Measuring the viscoelastic properties of human platelets with the atomic force microscope. *Biophys. J.* **70**, 556-567 (1996).

31. Needham, D. & Hochmuth, R. M. Rapid flow of passive neutrophils into a 4 microns pipet and measurement of cytoplasmic viscosity. *J. Biomech. Eng.* **112**, 269-276 (1990).

32. Evans, E. & Yeung, A. Apparent viscosity and cortical tension of blood granulocytes determined by micropipet aspiration. *Biophys. J.* **56**, 151-160 (1989).

33. Tran-Son-Tay, R., Needham, D., Yeung, A. & Hochmuth, R. M. Time-dependent recovery of passive neutrophils after large deformation. *Biophys. J.* **60**, 856-866 (1991).

34. Perrault, C. M., Bray, E. J., Didier, N., Ozaki, C. K. & Tran-Son-Tay, R. Altered rheology of lymphocytes in the diabetic mouse. *Diabetologia* **47**, 1722-1726 (2004).

35. Athanassiou, G., Matsouka, P., Kaleridis, V. & Missirlis, Y. Deformability and filterability of white blood cell subpopulations. Evaluation of these parameters in the cell line HL-60 and in type II diabetes mellitus. *Clin. Hemorheol. Microcirc.* **22**, 35-43 (2000).

36. Linderkamp, O., Ruef, P., Zilow, E. P. & Hoffmann, G. F. Impaired deformability of erythrocytes and neutrophils in children with newly diagnosed insulin-dependent diabetes mellitus. *Diabetologia* **42**, 865-869 (1999).

37. Nash, G. B., Johnson, C. S. & Meiselman, H. J. Mechanical properties of oxygenated red blood cells in sickle cell (HbSS) disease. *Blood* **63**, 73-82 (1984).

38. Glover, S. *et al*. Phosphorylation of focal adhesion kinase tyrosine 397 critically mediates gastrin-releasing peptide's morphogenic properties. *J. Cell. Physiol.* **199**, 77-88 (2004).

39. Yao, W. *et al*. Wild type p53 gene causes reorganization of cytoskeleton and, therefore, the impaired deformability and difficult migration of murine erythroleukemia cells. *Cell Motil. Cytoskeleton* **56**, 1-12 (2003).

40. Segal, M. S. *et al*. Nitric oxide cytoskeletal-induced alterations reverse the endothelial progenitor cell migratory defect associated with diabetes. *Diabetes* **55**, 102-109 (2006).

41. Veldkamp, C. T., Peterson, F. C., Pelzek, A. J. & Volkman, B. F. The monomer-dimer equilibrium of stromal cell-derived factor-1 (CXCL 12) is altered by pH, phosphate, sulfate, and heparin. *Protein Sci.* **14**, 1071-1081 (2005).

42. Hesselgesser, J. *et al*. Identification and Characterization of the CXCR4 Chemokine Receptor in Human T Cell Lines: Ligand Binding, Biological Activity, and HIV-1 Infectivity. *J. Immunol.* **160**, 877-883 (1998).

43. Voldman, J., Gray, M. L. & Schmidt, M. A. Microfabrication in biology and medicine. *Annu. Rev. Biomed. Eng.* **1**, 401-425 (1999).

44. Beebe, D. J., Mensing, G. A. & Walker, G. M. Physics and applications of microfluidics in biology. *Annu. Rev. Biomed. Eng.* **4**, 261-286 (2002).

45. Ratner, B. D., Hoffman, A. S., Schoen, F. J. & Lemons, J. E. Biomaterials Science: An introduction to materials in medicine, 2nd ed. (2004).

46. Xia, Z. Standard operating procedure: Silicon device fabrication process. (2004).

47. Gu, P. Personal communication (2009).

48. Smith, J. T., Elkin, J. T. & Reichert, W. M. Directed cell migration on fibronectin gradients: effect of gradient slope. *Exp. Cell Res.* **312**, 2424-2432 (2006).

49. Dow Corning. Information about Dow Corning® brand silicone encapsulants. (2008) www.dowcorning.com Accessed August 2009.

50. Schneider, F., Fellner, T., Wilde, J. & Wallrabe, U. Mechanical properties of silicones for MEMS. *Journal of Micromechanics and Microengineering* **18**, 065008 (2008).

51. Monahan, J., Gewirth, A. A. & Nuzzo, R. G. A method for filling complex polymeric microfluidic devices and arrays. *Anal. Chem.* **73**, 3193-3197 (2001).

52. White, F. in *Viscous Fluid Flow* (McGraw-Hill, Boston, 1991).

53. Chung, B. G., Lin, F. & Jeon, N. L. A microfluidic multi-injector for gradient generation. *Lab. Chip* **6**, 764-768 (2006).

54. Wheater, P. R., Burkitt, H. G., Stevens, A. & Lowe, J. S. Basic histopathology-A colour atlas and test. (1991).

BIOGRAPHICAL SKETCH

Jessica Ann Cobb received a Bachelor of Science degree, magna cum laude, in chemical engineering from Auburn University in May 2003. During her undergraduate career she was a member of the Honors College and was awarded the following scholarships: Auburn University Freshman Academic Scholarship, Amereda Hess Scholarship, and Chevron Texaco Scholarship.

In August 2003, Mrs. Cobb was awarded an Alumni Fellowship for graduate study in the Department of Biomedical Engineering at the University of Florida. She specialized in cellular and tissue engineering and worked under the guidance of Dr. Roger Tran-Son-Tay in the Cellular Mechanics and Biorheology Lab. In December 2004, she received a Master of Engineering degree. As she continued her studies in pursuit of a doctorate degree she was awarded an Auzenne Fellowship. She presented her work at three national scientific conferences and published a manuscript in a peer-reviewed journal.